RSC Advances

REVIEW

View Article Online
View Journal | View Issue

Cite this: *RSC Adv.*, 2022, **12**, 30985

Influence of VO_2 based structures and smart coatings on weather resistance for boosting the thermochromic properties of smart window applications

Muhammad Khuram Shahzad, *[a] Rana Zafar Abbas Manj,[b] Ghulam Abbas,[c] Rashid Ali Laghari,[d] Syed Sohail Akhtar,[de] Muhammad Aslam Khan,[a] Muhammad Bilal Tahir,[a] Sami Znaidia[fg] and Meshal Alzaid[h]

Received 26th July 2022
Accepted 28th September 2022

DOI: 10.1039/d2ra04661j

rsc.li/rsc-advances

Vanadium dioxide (VO_2)-based energy-saving smart films or coatings aroused great interest in scientific research and industry due to the reversible crystalline structural transition of VO_2 from the monoclinic to tetragonal phase around room temperature, which can induce significant changes in transmittance and reflectance in the infrared (IR) range. However, there are still some obstacles for commercial application of VO_2-based films or coatings in our daily life, such as the high phase transition temperature (68 °C), low luminous transmittance, solar modulation ability, and poor environmental stability. Particularly, due to its active nature chemically, VO_2 is prone to gradual oxidation, causing deterioration of optical properties during very long life span of windows. In this review, the recent progress in enhancing the

[a]*Institute of Physics, Khwaja Fareed University of Engineering and Information Technology, Rahim Yar Khan 64200, Pakistan. E-mail: khuram.shahzad@kfueit.edu.pk*

[b]*State Key Laboratory for Modification of Chemical Fibers and Polymer Materials, College of Materials Science and Engineering, Donghua University, Shanghai 201620, China*

[c]*Department of Physics, Faisalabad Campus, Riphah International University, Pakistan*

[d]*Interdisciplinary Research Center for Intelligent Manufacturing and Robotics, King Fahd University of Petroleum and Minerals, Dhahran, 31261, Saudi Arabia*

[e]*Mechanical Engineering Department, King Fahad University of Petroleum and Minerals, Dhahran, 31261, Saudi Arabia*

[f]*College of Sciences and Arts in Mahayel Asir, Department of Physics, King Khalid University, Abha, Saudi Arabia*

[g]*Laboratoire de Recherche (LR 18ES19), Synthese Asymetrique et Ingenierie Moleculaire de Materiaux Organiques pour l'Electroniques Organiques, Faculte des Sciences de Monastir, Universite de Monastir, 5000, Tunisia*

[h]*Physics Department, College of Science, Jouf University, P.O. Box: 2014, Sakaka, Saudi Arabia*

Dr Muhammad Khuram Shahzad was born in Chiniot, Pakistan, in 1986. He received his M.S. degree (2015) in Physics from the University of Agriculture Faisalabad, and his PhD degree (2019) in Physics under the guidance of Prof. Dr Yundong Zhang at Electronics Science and Technology building,, Harbin Institute of Technology, China. After graduation, he became an Assistant Professor in Khwaja Fareed University of Engineering and Information Technology (KFUEIT), Rahim Yar Khan, Pakistan, in 2021. Currently, he is working in the Institute of Physics, KFUEIT, Pakistan. His current research focuses on the synthesis of up-conversion nanomaterials, smart windows, 2D materials, DFT and its biological, sensor, energy applications.

Dr Rashid Ali Laghari is currently working as a post-doctoral research fellow at Interdisciplinary Research Center for Intelligent Manufacturing and Robotics, King Fahd University of Petroleum and Minerals, Dhahran, Saudi Arabia. His current research interests include FEA and predictive modeling and optimization of metal matrix composite material machining process, cutting simulation and machining process of titanium alloys, applied materials, manufacturing and computational mechanics, fabrication of metal matrix composite materials, and multi sensing IIoT platforms for process monitoring of CNC machines. He has authored/coauthored more than 25 publications and attended a number of international conferences.

thermochromic properties of VO_2-hybrid materials especially based on environmental stability has been summarized for the first time in terms of structural modifications such as core–shell structures for nanoparticles and nanorods and thin-films with single layer, layer-by-layer, and sandwich-like structures due to their excellent results for improving environmental stability. Moreover, future development trends have also been presented to promote the goal of commercial production of VO_2 smart coatings.

1. Introduction

Immense amount of energy is consumed every year to sustain thermal comfort in residential and commercial buildings, needing heat and air conditioning. All these processes lead to an increase in the consumption of electricity, CO_2 emissions, and the formation of huge amounts of air pollutants, including SO_2 and NO_2 emissions and particulate matter (PM_{10} and $PM_{2.5}$).[1–5] To alleviate these environmental problems, new advanced materials are needed to synchronize the transfer of energy for optimizing energy requirements. About 35% of the heat energy gets out through windows, leading to huge losses in energy.[6–8] Buildings (*i.e.*, the residence of modern humans) are among the utmost energy consumers and have a large impact on the environment. Buildings account for 39% of energy consumption in the USA and 40–45% in Europe.[9,10] The good news is that the capability for energy saving in buildings is also wide, if sharp energy-efficient technologies and designs are utilized.[11] Windows are essential for buildings for providing lighting and visual association with the outside world, and their existence demands much attention in advanced architecture. In terms of energy efficiency, simple windows are not playing a positive role due to some elements; windows regularly let in or let out a large amount of energy and add to energy consumption especially in summers and winters.[12] Therefore, as windows have a large effect on energy consumption/saving, they need to be made energy-efficient. Smart windows, which can be implemented in modern energy-saving buildings are currently being extensively investigated (coating with photochromic, thermochromic, and electrochromic materials).[13] Additionally, radiative cooling materials spontaneously radiate long-wave infrared (LWIR) to the cold outer space, providing cooling power that is preferred in hot seasons. Radiative cooling has been widely explored for walls and roofs but rarely for windows, which are one of the least energy-efficient parts of buildings. On-demand and selective regulation of radiative cooling (long-wave infrared, LWIR) and solar heat gain (ultraviolet, visible, near-IR, and UV-vis-NIR) of building facades is a grand challenge but essential to decrease energy usage in buildings.[14–16]

To expand the smart window technology, vanadium dioxide (VO_2) has attracted large attention due to its tunable different properties under the effects of external factors. Mostly, the common polymorphs are: VO_2(A) (tetragonal), VO_2(B) (monoclinic), VO_2(R) (tetragonal-rutile), and VO_2(M) (monoclinic-distorted rutile).[17] VO_2(A) is a metastable phase that occurs during the conversion of VO_2(B) into VO_2(R)[18] or VO_2(M),[19] depending upon the conditions of synthesis. Temperature sensing optical switching[20] and optical modulation and smart windows are all the areas of applications for the final device defined by the phase composition of the VO_2 powder or layers,[21] for example, Li-ion batteries and Na-ion batteries.[22–25] The phase structure of VO_2 is changeable depending upon the value of temperature, which is called the critical temperature ($T_c = 68$ °C). V. Wittwer and coworkers made the first observation of the semiconductor to metal phase transition in VO_2.[26] Below 68 °C VO_2 changes to the monoclinic from tetragonal phase, having transmittance properties instead of the reflection of infrared radiation, but it remains lucid to the visible range of radiation. Phase transition and functional properties such as morphology and dimensionality,[27] stoichiometry, doping,[28–30] and type of lattice (low-temperature phase) are now commonly discussed. On the basis of these properties, thermochromic windows can efficiently reduce energy consumption in residential and commercial buildings because phase transitions successfully adjust solar irradiation in the wavelength region of 800–2500 nm.[31–35] Based on these properties, VO_2 represents a promising active material in the field of energy-efficient smart windows.

Nevertheless, there are still many hurdles for commercial applications as smart coatings on energy-efficient fenestrations, which seriously limit the relative usefulness of VO_2 smart coatings. (i) The phase transition temperature (T_c) of pure bulk VO_2 (at 68 °C) is mostly applicable on building fenestrations when a T_c of about 40 °C is considered appropriate; (ii) VO_2 coatings' relative modulation capabilities are not much efficient to save energy due to the fact that the modulation of VO_2 for sun oriented radiation is mostly relegated to the transmittance

Dr Syed Sohail Akhtar currently holds the rank of Professor in the Department of Mechanical Engineering at King Fahd University of Petroleum & Minerals (KFUPM). His research areas are applied materials, manufacturing, and computational mechanics focusing on a mix of futuristic and present-day research that is of practical significance and has immediate relevance and impact in the industry. He has authored/co-authored more than 100 archival technical publications, including more than 90 ISI journal papers, and published 02 books, and many book chapters. He presented his research at several international conferences as an invited speaker. In collaboration with other research fellows, he worked on more than 20 basic and applied research projects; some of them were internally funded by the KFUPM, while others were funded by external agencies and institutes.

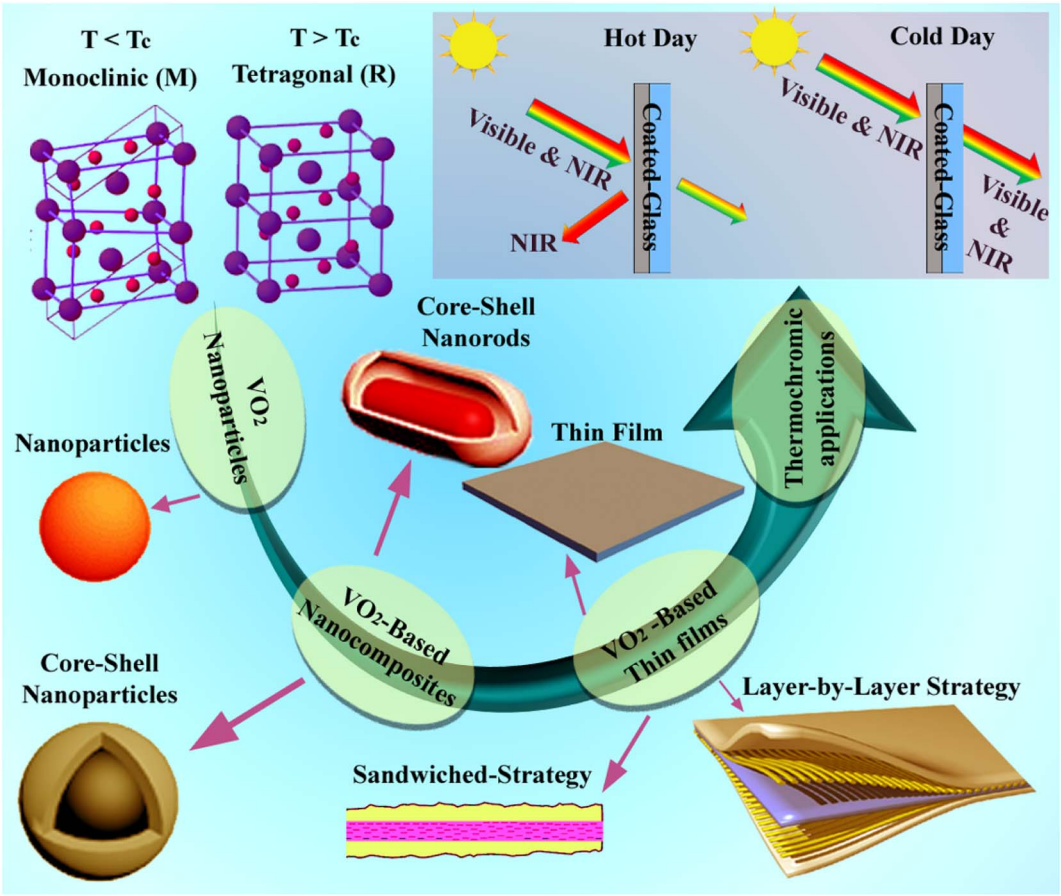

Scheme 1 Overview of VO_2-based composites on durability against a harsh environment.

switch within the near-infrared region, which is accounted for 43% of sun powered vitality within the sun oriented spectrum; (iii) the glowing transmittance T_{lum} for a single layer of VO_2 with alluring ΔT_{sol} is, as a rule, less than 40% (indeed 30%) due to retention within the short-wavelength region extending in both the semiconducting states and metallic states of VO_2, which is anticipated to exceed by at least 50% for regular applications; (iv) as an advanced coating, VO_2 must maintain good thermochromic performances for at least a decade for practical applications.[36–39]

However, in the real environment, VO_2 finally changes to the V_2O_5 phase, which is the most thermodynamically stable phase.[40–42] Considering, the environmental conditions, VO_2, could be an awesome challenge for general applications such as modern coating. These challenges must be solved for practical applications to be realized, and various attempts have begun to accomplish this goal. Distinctive strategies have been proposed to solve these issues including doping with different particles in a viable way to tweak the phase-transition temperature of VO_2,[43–45] multilayer structures,[46,47] nanocomposites, and manufacturing nanostructures to enhance the optical properties,[48–50] counting improving solar-modulation abilities and progressing better luminous transmittances. Many works have used these tactics which have been detailed in earlier reviews.[51–55]

Unfortunately, except for the above-mentioned hindrances there exist new but critical challenges for VO_2 based coatings that may have been overlooked in the foregoing work. The constraints of VO_2 based smart coatings are presented in this review, to address these difficulties, merging current research with future possibilities. Furthermore, as researchers' interest in this topic has grown, this work highlights broad evaluation standards that can be used to compare qualities objectively. In this review, we have focused on thermochromic VO_2 smart coatings for enhanced thermochromic performance, environmental stability, and mass production for commercial applications on building fenestrations. With the development of material fabrication technology, various VO_2 nanostructures, *e.g.*, thin films and low-dimensional structures (LDSs), have been successfully fabricated and have been widely investigated to enhance environmental stability in thermochromic smart windows, as shown in Scheme 1. Thin films and LDSs are suitable for micromachining processes, which promotes the development of both macro and micro-scale devices. As we know, the metal-insulator transition (MIT) temperature and behavior of VO_2 are extremely sensitive to external stimuli, including doping, strain, surface/interface effects, electrochemical gating, electric field, light, electron beam, *etc.* Besides, the morphology also has a great influence on the properties of the VO_2 material. VO_2 LDSs-nanowires (NWs), nanodots (NDs),

nanoparticles (NPs), nanorods (NRs), nanobelts (NBs), nanosheets (NSs), *etc.* exhibit unique electrical, mechanical and optical properties different from their bulk counterparts due to the size and surface/interface effects. Thus, we categorized the literature based on structures such as coatings in the form of core–shell structures for nanoparticles and nanorods, and thin-films, which led to the layered and layer-by-layer and double-layer structures, *etc.* The coating layers of various materials on VO_2 particles played an outstanding role to enhance the durability of hybrids by preventing the direct contact between air and VO_2 particles, which led to the improvement of the thermochromic performance (T_{lum} and T_{sol}) of VO_2 and its hybrids. On the basis of a survey of excellent experimental works on VO_2, we aim to provide a wide range of insights into the recent studies in the above mentioned field.

2. Structures of VO_2 for durability

The unstable behavior of VO_2 particles is the major problem for their practical application in smart windows. The stabilization of VO_2 has been deemed a key factor for realizing the outstanding candidate for smart window applications. To improve the structural integrity of active materials in various fields, surface modification remained an excellent strategy through different structures of active materials. However, the surface modification of VO_2 also has huge potential for improving its stability against a harsh environment by avoiding the direct contact between air and the surface of VO_2 particles. As a result of the prevention of direct contact with air, the durability of thermochromic performances of VO_2 is significantly enhanced, which is summarized below.[56–60]

2.1 VO_2 nanoparticle-based core–shell structures

In the core–shell structure strategy, the shell materials provide the protection of the core from various factors such as oxidation, harsh environments, and produced stress in the core materials. Because of the synergic effects of the core–shell structure, the composites emerge with excellent properties instead of intrinsic properties of core materials. As a result of the combined properties of core materials and modification, the composites deliver excellent performances in practical applications.[61–65] VO_2 particles have been used as core materials to evaluate the performance in smart window applications. Y. Chen and coworkers presented the fabrication of VO_2@ZnO core–shell nanoparticles, which improved the stability of VO_2-based films in practical architecture (Fig. 1(a)).[66] In the entire process of forming a VO_2-based film, the transmission electron microscopy (TEM) image exhibits that nanoparticles were covered with a ZnO shell with a thickness of roughly 20 nm as seen in Fig. 1(b). Furthermore, the durability of VO_2-based smart windows was significantly improved by VO_2@ZnO core–shell structures. The coated shell acted as a barrier to the flow of oxygen and water. It prevented the oxidation of VO_2 to V_2O_5. They created a harsh atmosphere with a constant temperature of 60 °C and a humidity of 90%. The degree of decline in thermochromic performance was used to assess the durability of VO_2-based films. They analyzed the transmittance spectra of an uncoated VO_2 film and VO_2@ZnO film. After 12 hours, the transmittance contrast between the low-temperature semiconductor phase and high-temperature phase in the uncoated VO_2 film began to decrease. For the uncoated VO_2 film, the ΔT_{sol} was 17.2% within the initial state and decreased to 0% after 30 h. It is evident through Fig. 1(c) and (d) that the organized VO_2@ZnO nanoparticles primarily based for smart windows totally demonstrated strong sun modulation efficiency, excessive luminous transmittance, and fantastic sturdiness in a hot, humid, and oxygenic environment. It could well be found that the transmittance contrast between 20 and 80 °C at $\lambda = 1500$ nm ($\Delta T_{\lambda} = 1500$) started to decrease with the time increasing. S. Zhao and coworkers applied an inorganic–organic hybrid lined of VO_2 nanoparticles for more advantageous durability.[67] They proposed a VO_2@MgF_2@polydopamine (PDA) inorganic–organic hybrid. Fig. 1(e) shows the synthesis process of VO_2@MgF_2@PDA. The coated architecture greatly enhances the optical durability more than 13 times in contrast to pristine VO_2 and the transmittance difference between room and high temperature changed within 20% (decreasing from 25 to 20.1%) at $\lambda = 1200$ nm after an ageing time of 1000 h at constant temperature (60 °C) and relative humidity (90%). The SEM image can be seen clearly from Fig. 1(f). It depicts the representative core–shell structure. For the durability portrayal of inorganic core–shell nanoparticles, temperature-responsive optical films were ready and positioned in a soggy warming environment ($T = 60$ °C, RH = 90%) for testing their optical properties in a predetermined time frame. After different aging times, the visible infrared (vis-IR) transmittance of VO_2 nanoparticles demonstrates the durability of VO_2@MgF_2 core–shell architectures. It is observed that it was worse than the VO_2 core only. The hydration effect of the VO_2 core surface in the core-preparation process could be the reason. Further, the VO_2 nanoparticles can be damaged after many days of soaking in water and the disassembling process can accelerate if the pH of water is not neutral. Fortunately, the durability of VO_2@MgF_2 has been increased by almost ~6.5 times (from 77.5 h to more than 500 h) in EG solvent. Under the same conditions as VO_2@MgF_2, the optical durability of VO_2@MgF_2@PDA inorganic–organic core–shell nanoparticles is presented in Fig. 1(g). The durability has substantially improved after PDA coating and the value of ΔT changed by 20% (from 25 to 20.1%) after 1000 hours of treatment at constant temperature (60 °C) and humidity (90%). In comparison to pristine VO_2 (the durability time is higher than that of others) the durability time of VO_2@MgF_2@PDA has been increased by more than 13 times. The differential scanning calorimetry (DSC) curves of VO_2@MgF_2 have the endothermic peak at 64.1 °C in the heating process and the exothermic peak at 41.3 °C in the cooling process, as illustrated in detail, and it showed that the DSC cycle corresponds to one cycle of high–low–high transmittance. Bifunctional template-induced VO_2@SiO_2 Dual-Shelled Hollow Nanosphere-based coatings (DSHNs) were prepared by Z. Qu and coworkers.[68] They investigated the thermochromic and optical performances of VO_2@SiO_2 DSHN coatings; a UV-vis-IR spectrophotometer with the assistance of the warming stage

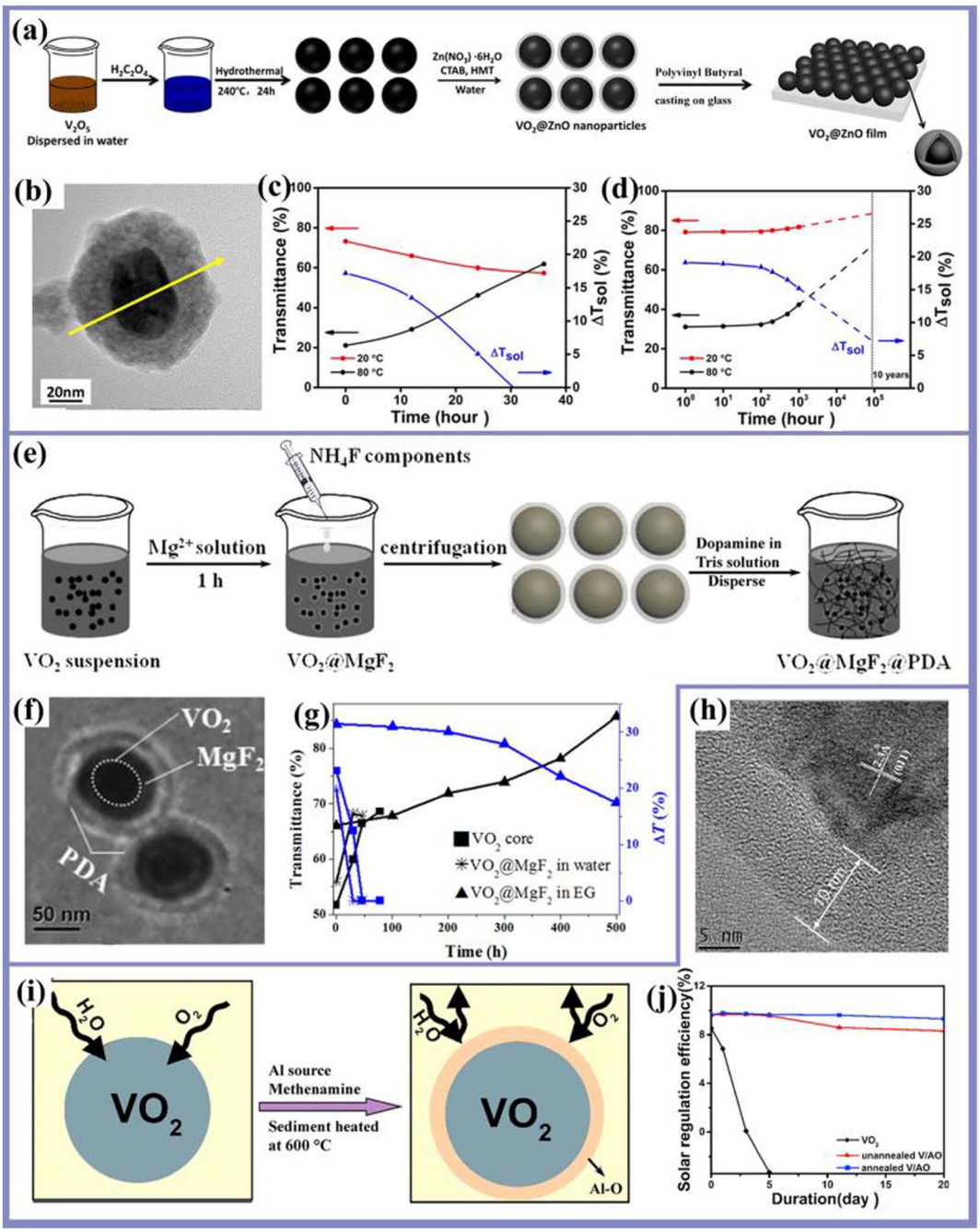

Fig. 1 (a) Experimental flow chart for the synthesis of VO_2@ZnO core–shell structure nanoparticles and VO_2@ZnO films. (b) TEM images of VO_2@ZnO core–shell structure nanoparticles. Optical transmittance spectra of (c) uncoated VO_2 and (d) VO_2@ZnO. Reproduced with permission[66] copyright © 2017, American Chemical Society. (e) Flow chart for the whole process of flexible film preparation and influence of reaction parameters for depositing MgF_2 on the surface of the VO_2 core. (f) TEM images of VO_2 nanoparticles with different shell thicknesses of VO_2@MgF_2. Vis-IR transmittance spectra of the VO_2 core. (g) Curves of visible light transmittance and the transmittance difference (ΔT) between room and high temperature at $\lambda = 1200$ nm of these samples with the change of treatment time. Reproduced with permission[67] Copyright © 2019, American Chemical Society. (h) SEM image of the sample. (i) Preparation of VO_2 and AlO. (j) Transmittance spectra with different time spans. Reproduced with permission[69] Copyright © 2017, Elsevier.

was used to quantify the temperature-dependent transmittance. The test results and the determined optical performances (T_{lum} and ΔT_{sol}) are examined in detail. Concentrating with the nonstop and dense VO_2 coatings, the VO_2@SiO_2 DSHN coatings introduced much better optical work. With the rise of the refluxing time, the T_{lum} increased from 42.5% to 66.3% (VS1) first and then, at that point, decreased to 61.7% (VS2) and 61.8% (VS3), separately. Meanwhile ΔT_{sol} expanded from 7.6% to 10.7% (VS1), 10.5% (VS2), and 12.6% (VS3), independently. The RI of VO_2@SiO_2 DSHN coatings gained in the current work

exhibited a dramatic reduction, and reached 1.63 at a wavelength of 630 nm, diffusing the coating with the best anti-reflection (AR) effect. They also matched the transmittance spectra at low temperature by finite-difference time-domain (FDTD) using the measured optical constants. It is found that the calculated results are in strong accordance with the experimental spectra. Consequently, the dual-shell hollow nanoparticles of VO_2@SiO_2 demonstrated extraordinary potential in enhancing the optical performance of thermochromic coatings. K. Tong and coworkers synthesized VO_2 nanoparticles covered with Al–O-based shell (V/AO) nanoparticles by utilizing a facile method.[69] The strengthened V/AO nanoparticles had shown great durability for the unique environment. TEM images can be seen in Fig. 1(h); it showed the typical structures of the annealed V/AO nanoparticles in a better way. Moreover, Fig. 1(i) represents the VO_2 nanoparticles that had directly reacted with water and oxygen. The reaction had begun at the outer layer of the VO_2 nanoparticle, and V^{4+} had oxidized to V^{5+}. Subsequently, the VO_2 no longer has the thermochromic property but an un-annealed Al–O-based shell allowed for a shelter to the VO_2 center, which delayed down the diffusion of water and oxygen into the VO_2 cross section. The un-annealed (V/AO) nanoparticles reliably decreased the thermochromic property. The annealed (V/AO) nanoparticles outlined the preferred stability over un-annealed (V/AO) nanoparticles because the previous shell had more excellent compactness and gave sufficient protection for the core. Further, shell of Al–O-based to the VO_2 center, the stability of the thermochromic nanoparticles, is estimated and put into a climate chamber to replicate the result of humidity and temperature. The annealed Al–O-based shell had shown the most stability of the VO_2 core. The transmittance of the films had been estimated around the same value. It showed the progression of ΔT_{sol} for different values. The annealed V/AO nanoparticles explain the most generous stability of three samples, with ΔT_{sol} changing from 9.62% to 9.30% after 20 days of aging, which indicates that the

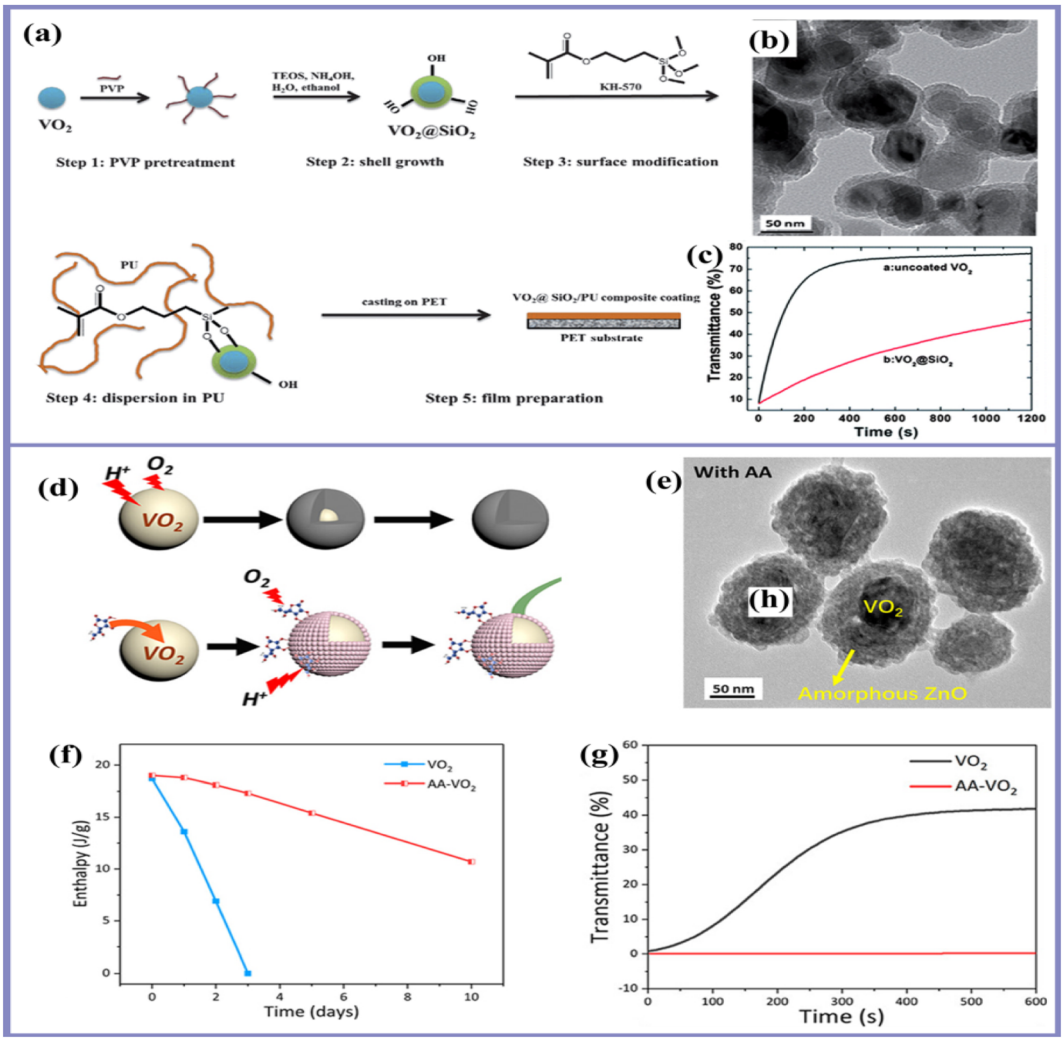

Fig. 2 (a) Preparation procedure for VO_2@SiO_2 nanoparticles and flexible composite films. (b) TEM images of the VO_2@SiO_2 composite film. (c) Transmittance spectra of coated and un-coated samples. Reproduced with permission[74] Copyright © 2012, The Royal Society of Chemistry. (d) Preparation process of VO_2 and AA-VO_2. (e) TEM images of VO_2 nanoparticles and AA-VO_2. (f) Transmittance spectra with time in days. (g) Transmittance spectra with time in seconds. Reproduced with permission[76] Copyright © 2019, American Chemical Society.

annealed Al–O-based shell is compact and blocks the diffusion of moisture and oxygen more effectively. So the annealed V/AO nanoparticle had the capacity for the broad application of the VO_2-based thermochromic film. Fig. 1(j) reveals that VO_2 nanoparticles had been secured by the Al–O shell and stayed stable when placed in a damp warming climate. The temperature of VO_2 only shows high at (350 °C in the air) which assure the presence of the Al–O-based shell. These core–shell structure nanoparticles had shown good optical properties and chemical stability. The shell had a successful boundary layer to keep away from oxygen and water from diffusing into the VO_2 materials. So, VO_2 is protected by the Al–O-based shell and applied in smart windows, such as automobiles, buildings, *etc.* It was found that the above mentioned techniques are suitable for durability-enhancement against weather resistance of smart window applications.

The coatings of metals as a shell on different core materials have shown extraordinary results in various applications.[70–73] By taking the advantages of different coating materials, Y. Gao and coworkers used the dip-coating technique to create transparent flexible hybrid VO_2-based films with exceptionally high thermochromic characteristics as shown in Fig. 2(a).[74] Fig. 2(b) displays the TEM images of the original VO_2 nanoparticles and the silica-coated VO_2 nanoparticles with a PVP prepared sample. PVP pre-treatment favored the production of smooth, uniform silica shells. PVP is an amphiphilic polymer, which could keep the nanoparticles stable in water and a variety of non-aqueous solvents. The transmittance spectra of coated and uncoated samples after various acid exposure times are shown in Fig. 2(c). After the first 200 seconds, the uncoated particles had a quick 56.2 percent rise in transmittance, from 8.6% to 64.8%. The coated particles experienced an increase of 10.9%, from 8.1% to 19.0%. This result exhibits that VO_2@SiO_2 was able to confront the acidic treatment due to the protection of the SiO_2 shell. The films had great flexibility and fair visible transmittance due to the above mentioned results. Generally optical transmittance of spectra and thermal hysteresis loops are presented at the wavelength of 1500 nm of films. J. Zhu and coworkers tried to prepare $V_xW_{1-x}O_2$(M) NPs, which were subsequently coated with a thin layer of silica, shielding VO_2 NPs from aggregating and forming during the annealing process.[75] The production process of $V_xW_{1-x}O_2$(M)@SiO_2 and nano-crystal coated VO_2 with SiO_2 materials is discussed. They presented the TEM pictures of the VO_2(M)@SiO_2 and the annealed VO_2(M)@SiO_2 nano-materials. It was noted that essentially every single VO_2 nanoparticle was coated with a SiO_2 shell independently. The crystallinity of VO_2 nanoparticles was essential for the best thermochromic execution of vanadium dioxide-based thermochromic smart coating (VTSC). They addressed the transmittance spectra of VTSC based on the prepared particles. Both the silica coating and annealing showed excellent effects on the thermochromic properties. The T_{lum} and ΔT_{sol} were increased from 56.6% and 8.7% to 59.7% and 11.3%, respectively, after the original VO_2(M) NPs were coated with a layer of silica. The thermochromic performance was good enough to obtain VTSC suitable for practical construction. Y. Chen and coworkers prepared the core–shell structure by applying the ascorbic acid shell on VO_2 nanoparticles and measured the thermochromic properties for smart window application (Fig. 2(d)).[76] The covalently bonded ascorbic acid shell played an outstanding role to uplift the durability and anti-oxidation properties of VO_2 by avoiding further oxidation with air, which became fruitful for enhancing the life span of VO_2 in a humid environment. Transmittance spectra of the ascorbic acid-coated sample and

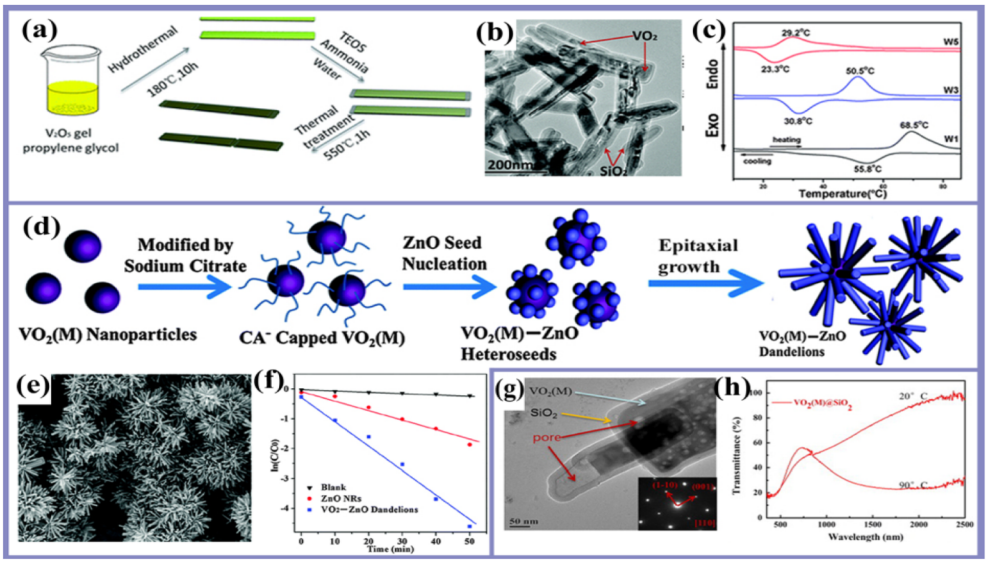

Fig. 3 (a) Experimental flow chart for the synthesis of the vanadium dioxide rod structure. (b) SEM images of VO_2@SiO_2 rod structure nanoparticles. (c) *Exo* and *endo* curves with different temperatures. Reproduced with permission[81] Copyright © 2013, The Royal Society of Chemistry. (d) Flow chart for the whole process of VO_2(M)–Zno dandelions. (e) TEM images of VO_2(M)–Zno dandelions. (f) Thermochromic graph at different times for Zno nanoparticles and VO_2–Zno. Reproduced with permission[82] Copyright © 2016, The Royal Society of Chemistry. (g) SEM images of pore, VO_2(M) and SiO_2. (h) Transmittance spectra of VO_2(M)@SiO_2. Reproduced with permission[83] Copyright © 2013, Elsevier.

uncoated sample were compared. It delivered excellent anti-corrosion properties in H_2SO_4 and H_2O_2 environments, which led to enhance the thermochromic properties. Ascorbic acid remained firmly on VO_2 particles due to strong interfacial interaction between VO_2 particle surfaces and ascorbic acid coating, which was confirmed by SEM (Fig. 2(e)). It was found that the thermochromism of pure VO_2 completely vanished within 3 days due to phase changes, but coated VO_2 remained stable and the thermochromic property existed without phase changes against a humid environment. The result can be easily observed in Fig. 2(f). The durability of ascorbic acid-coated VO_2 was also investigated under a highly humid environment (humidity 90% and temperature 60 °C) through differential scanning calorimetry in Fig. 2(g). This method provides a promising way for weather resistance applications.

2.2 VO_2 nanorod-based core–shell structures

The nanorod structure core exhibits a remarkable modulation ability for thermochromic and solar infrared light. Nanorod structures with both thermochromic and photocatalytic properties offer significant potential for creating a multifunctional smart coating. Thus, nanorods have proved to be the best for structural modification compared to spherical particles for various applications and have gained huge attention because of the best shape anisotropy. The good physical properties of nanorods could mostly be achieved by using different metals. Considering the advantages of nanorods, this structural modification of VO_2 with a core–shell structure has also been tried in smart window applications.[77–80] For example, A. Huang and coworkers arranged $V_xW_{1-x}O_2$(M)@SiO_2 ultra-thin nanostructures.[81] They had prepared ultra-thin VO_2(B) nanostructures with a diameter of approximately 15 nm by a simple post-annealing method, and the VO_2(M) nanoparticles were obtained in this process as shown in Fig. 3(a). The arranged VO_2(M) and VO_2(M) execution show that the VO_2(M) nanoparticles that is required excessive temperatures and longer times with the assistance of the hydrothermal process. Fig. 3(b) clearly demonstrates the TEM images of the prepared VO_2@SiO_2 sample and SiO_2 had an external shadow portion and the inside darker section had VO_2. The presence of the silica shell had greatly enhanced the anti-oxidation ability of the VO_2 powders and had subdued nanoparticles throughout the

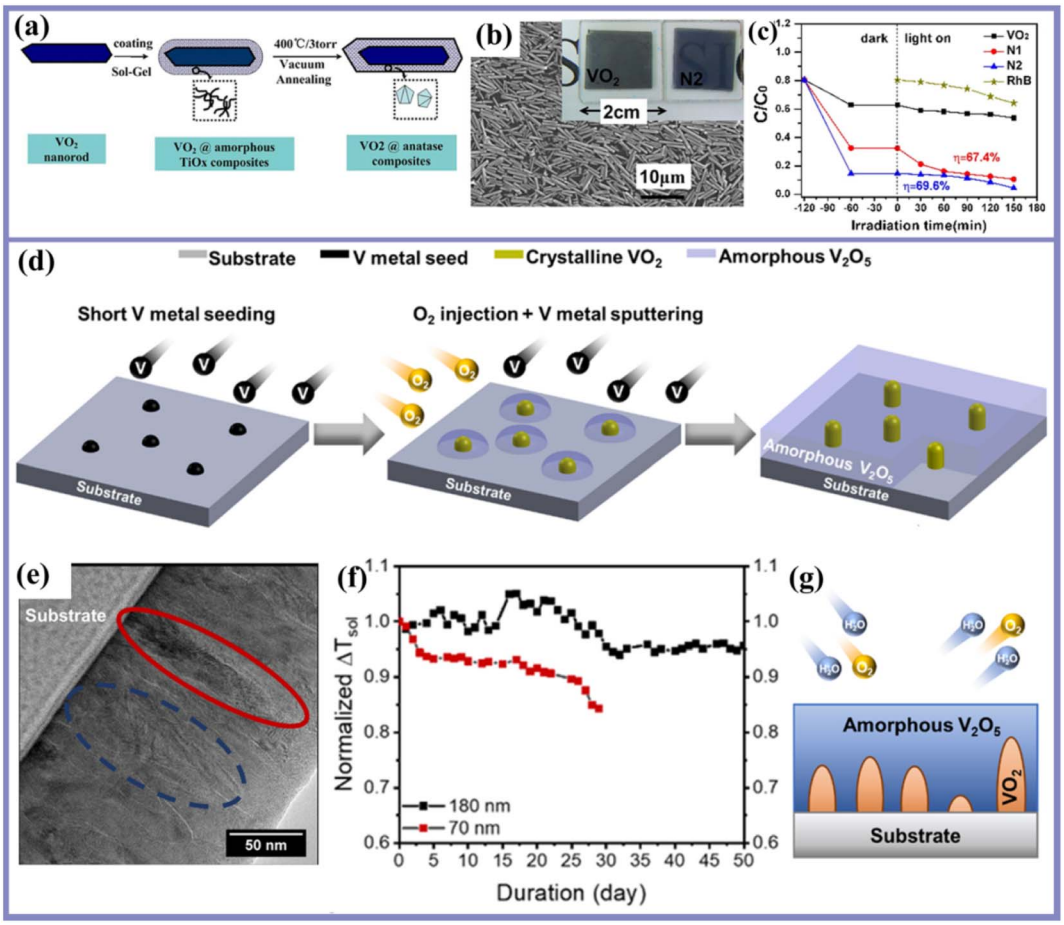

Fig. 4 (a) Preparation of the VO_2@anatase composite. (b) SEM images of the VO_2@anatase composite. (c) Transmittance spectra of VO_2@-anatase. Reproduced with permission[84] Copyright © 2013, The Author(s). (d) Preparation of V_2O_5/VO_2 seeding *via* a one-step high-powered impulse magnetron sputtering process. (e) SEM images of the amorphous V_2O_5 matrix. (f) Transmittance spectra of V_2O_5/VO_2. (g) Amorphous V_2O_5/VO_2 process. Reproduced with permission[85] Copyright © 2022, Elsevier.

thermal method. However, the luminous transmittance increases with the SiO_2 shell because it had a transparent structure. It simply represents that T_c had decreased with increasing the amount of doping at 20 °C. The optical transmittance spectra of the as-arranged VO_2(M)@SiO_2 nano particles with various amounts of W-doping (W1, W3, and W5) at low temperature (20 °C) and high temperature (90 °C) were discussed. When the measured value of W-doping expanded, T_{lum} diminished moderately due to an increase of the free-electron density, which was related to the increase in the absorption and reflection of visible light at previously mentioned below temperature. The top free electron density narrows the VO_2(M) energy gap in the semiconductor case. It reduced the value of enthalpy VO_2(M/R) *via* the phase transition of ΔT_{sol}. Due to dispersion and addition of the inert silica coating in the optical transmittance spectra, T_{lum} was increased from 15.73% to 24.69%. ΔT_{sol} was improved from 4.6% to 7.15% due to the anti-reflection of SiO_2. The most beneficial and accurate method is *via* W-doping, which was done in this sample, as seen in the DSC curves (Fig. 3(c)). W. Li and coworkers fabricated VO_2(M)–ZnO heterostructured dandelions.[82] Fig. 3(d) elaborates the mechanism of the VO_2(M)–ZnO, which was used to examine the dandelions, and three different samples were synthesized for ZnO NR measurements, VO_2(M)–ZnO without Na-CA and VO_2(M)–ZnO without ZnO seeds. The scanning electron microscopy (SEM) image displayed that the samples comprised ZnO and VO_2(M), as seen in Fig. 3(e). The reversible stages of the transition temperature of the pure VO_2(M) and VO_2(M)–ZnO composite powders were demonstrated by using differential scanning calorimetry (DSC). Moreover, Fig. 3(f) demonstrates that the ZnO NRs were consistently propagated on the surface of the VO_2(M) NPs to develop the VO_2(M)–ZnO hetero-junction because of interfacial contacts. Following recreated sunlight irradiation, the electrons and holes were photo-generated to save separately. The enhanced thermochromic features and chemical stability were associated with the ZnO. The composite film of VO_2(M)–ZnO showed a diminished stage transition temperature (T_c = 62.6 °C) with an increasing visible transmission ($T_{vis\text{-}l}$ = 52.2%) and solar modulating ability (ΔT_{sol} = 9.3%) as contrasted with the pure VO_2(M) film. R. Li and coworkers prepared vanadium dioxide (M)@SiO_2 NPs.[83] The rectangular parts of VO_2(B) nano-plates with a diameter ranging from 20 to 30 nm were hydrothermally manufactured, and the VO_2(B)@SiO_2 core–shell structure was made by utilizing an advanced Stober technique; Fig. 3(g) represents the thin layer of SiO_2 (30 nm) that was homogeneously surfaced on VO_2(M). In particular, the nano-pores showed two particular sizes: more prominent ones lied at the interface between VO_2(M) and SiO_2, and shorter ones laid inside the VO_2(M). Significantly, different nano-pores were made inside VO_2(B)@SiO_2 nanoparticles because of the variety in thickness between VO_2(B) and VO_2(M), which was given by higher optical transmittance and thermal protection. The optical transmittance of VO_2(B)@SiO_2 in comparison to VO_2(M) was discussed. It was noticed that VO_2(M) showed a sharp optical distinction between the high and low-temperature phases, indicating the single-phase characteristic and high crystallinity of the VO_2(M) film. VO_2(B)@SiO_2 exhibited a vastly improved optical performance with a higher visible transmittance and a more extensive solar modulation process, which was observed by the corresponding spectra in Fig. 3(h). The given data were contrasted to the obvious transmittance of 31.72% for VO_2(M), and the VO_2(B)@SiO_2 exhibited an obvious transmittance of 35.96%, with an increment of 13.4%.

Y. Li and coworkers synthesized the VO_2@TiO_2 core/shell nano particles as seen in Fig. 4(a).[84] Fig. 4(b) expresses the SEM images of TiO_2 shell composites. It also depicts the behavior of the VO_2@anatase composite. Moreover, Fig. 4(c) presents the dark and light on graph. The transmittance curves exhibited an un-doped VO_2 process after preparation of a layer, and the average transmittance was improved with the deteriorated modulation technique. And the loop width was also down by 5.7 °C. The above mentioned methods depicted good thermochromic performance against weather resistance potential for practical application of VO_2-based smart windows. T. D. Vu and coworkers reported a new strategy of nanocompositing vanadium dioxide preparation with excellent durability.[85] They employed the glass industry compatible process of magnetron sputtering, followed by rapid thermal annealing (RTA). Instead of the usual continuous films, this thin film process gave a unique structure where VO_2 NPs are dispersed in a V_2O_5/V_3O_7 matrix with a dense thermodynamically stable V_2O_5 overcoat. The key factor that allows for the deposition of nanorod VO_2 embedded inside the V_2O_5 matrix is the introduction of seeding, followed by delayed injection of O_2. As shown in Fig. 4(d), the sputtering process is divided into two phases. The first phase is the seeding of vanadium on the substrate. In this phase, the isolated island of vanadium nucleus is formed through the sputtering of the vanadium metal target for a short duration of 10 s in this study. At the end of the seeding phase, O_2 is slowly injected into V metal. The SEM image shows the presence of V metal seeds and crystalline VO_2 behaviour. It can be seen clearly in Fig. 4(e). This new type of nanocomposite gives a nearly doubled ΔT_{sol} (20%) compared with that of the best reported continuous single vanadium oxide film (10%) and high duration as seen in Fig. 4(f). The accelerated test suggested that the expected service life of this film is 23 years, which is a breakthrough in VO_2 based thermochromic smart windows. Fig. 4(g) depicts that the VO_2 nanorod structure is formed by introducing seeding guided growth along with manipulation of gas injection timing and target current during reactive sputtering, resulting in the V_2O_5/VO_2 thermochromic composite film. The high durability, due to the encapsulation of V_2O_5, together with the significantly enhanced thermochromic properties and facile industry compatible process, provides a new strategy to scale up this technology into real-world applications.

Combining VO_2 particles with polymers and two dimensional materials is deemed to boost the thermochromic properties of VO_2-hybrids for long term durability.[86–90] W. Li and coworkers arranged useful fiber mats with tunable diffuse reflectance and VO_2/PVP composite fiber mats.[91] The VO_2/PVP composite fibers were scattered by the inter-fiber scattering process, which means light phenomena. Every scattering process involved absorption and reflection was due to the

dispersion of the incident light. The absorption expanded to understand the absorption coefficient of VO_2 nanoparticles, and the cross-sectional of these fibers was modified to investigate the optical property. The VO_2 and W doped VO_2 nano particles were phase-stable. The diffraction peak shift created by W doping was apparent in the nanoparticles immersed in PVP. They showed that the W-doped VO_2 nano particles consisted of the diffuse reflection spectrum of fiber mats. They tuned their temperature phase transition in to 40 °C and its diameter was 800 nm that exhibited the diffuse reflection range by the blue line in the infra-red range. The diffuse reflectance demonstrated that no variation existed above 68 °C, which was more than that of the fiber mat included 0.05 g of VO_2, then the appropriate diffuse reflection property associated with VO_2 particles. J. Zhou and coworkers arranged nano-scale VO_2 and performed characterization of VO_2(M)–SnO_2 thermochromic films, and annealing was utilized to change over them into VO_2(M)/SnO_2 hetero-structures.[92] The optical band gap of the VO_2 crystals was expanded. Thus, the optical properties were enhanced. The nanosized particles (SnO_2) are bigger as compared to outer layer of the VO_2(M). They showed the reversible phase transition temperature of the VO_2(M) and VO_2(M)/SnO_2. It was concluded that the sharp endothermic peak of the pure VO_2(M) was determined at 73.7 °C, which was marginally bigger than 68 °C. Yet, the phase transition temperature of the VO_2(M)/SnO_2 hetero-structure was decreased from 69.8 °C. The change between endothermic and exothermic peaks for the VO_2(M)/SnO_2 hetero-structure was 9.6 °C, which was a lot lower than the 15.9 °C of the pure VO_2(M). It was seen that the loop amplitude of the VO_2(M)/SnO_2 hetero-organized film was 10.7 °C, which was limited by 7.1 °C related to the pure VO_2(M) film. The limited hysteresis has raised the affectability of phase transition responses to the different values of temperatures. They demonstrated the optical transmittance spectra and the corresponding film images. The optically improved performance of nano-sized SnO_2 on the surface of exposed VO_2 nano-rods yielded better results. The above mentioned results have expressed the best performance of weather resistance of smart window applications.

2.3 Thin film strategies of VO_2 at the device level

2.3.1 VO_2-based thin film structures. The layer by layer thin film preparation strategy is one of the simplest and most effective methods for preparing thin films. Compared with mixing film-growth techniques, layer by layer preparation of thin films provides better control of the structure at the molecular level.

The coating of materials on VO_2 particles at the nanoscale level is considered an expensive method of fabrication at the industrial level. The structural modification based on the thin film is the easiest and cheapest process for coating at a bulk level, which may affect the cost of the final product.[93–100] The thin film coating has also been investigated by combining different materials through various methods. For example, by a simple mixing method, a thin film has been tried by J. Sang and coworkers, in which they achieved the VO_2–ZnO combined films with improved thermochromic features by a facile ball-

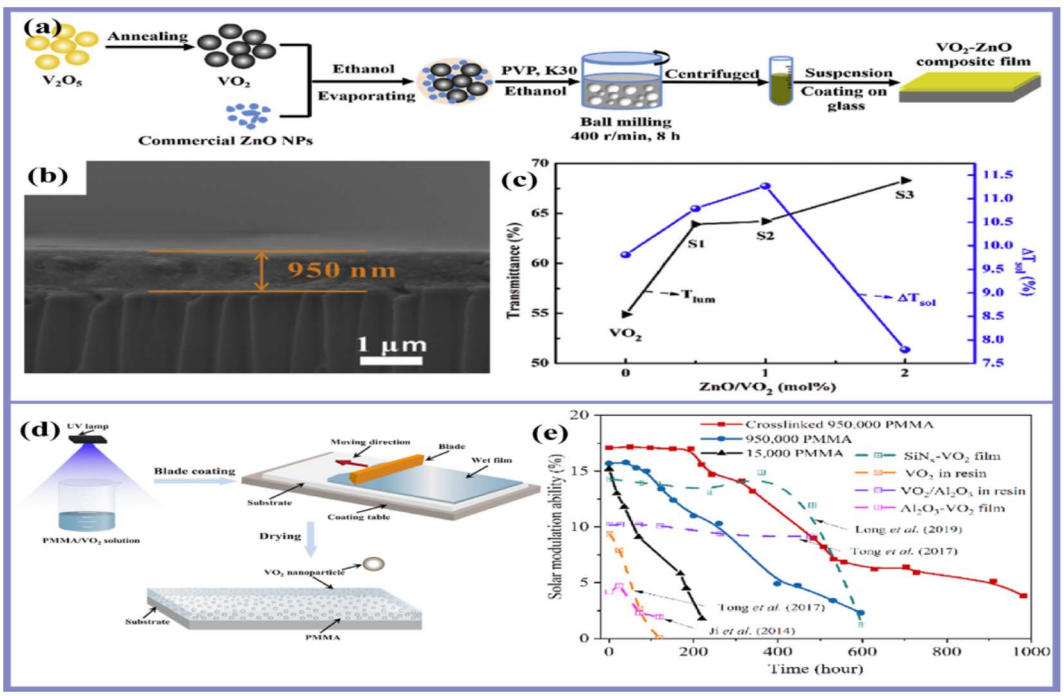

Fig. 5 (a) Experimental flow chart for the synthesis of VO_2@ZnO core–shell structure nanoparticles and VO_2@ZnO film. (b) TEM images of VO_2@ZnO core–shell structure nanoparticles. (c) Optical transmittance spectra of VO_2@ZnO at a constant temperature (60 °C) and humidity (90%). Reproduced with permission[101] Copyright © 2019, Elsevier. (d) Flow chart for the whole process of VO_2@PMMA film preparation. (e) Solar modulation of the VO_2@PMMA film. Reproduced with permission[102] Copyright © 2020, Elsevier.

milling method.[101] Fig. 5(a) depicts the facile ball-milling method by which VO_2–ZnO composites were made, and the combined films were built. The morphology of the as synthesized sample was presented by the SEM image as seen in Fig. 5(b). The ZnO NPs were represented as a scattering medium that was consistently filled in the space between the VO_2 powders throughout the process of ball milling. The ZnO NPs were added to optimize the thermochromic properties of the VO_2. The addition of ZnO uniformly increased the thermochromic properties, and its excellent performance was achieved, having results of T_{lum} = 64.2% and ΔT_{sol} = 11.3%. Moreover, the film coated with two layers displayed an ultra-high ΔT_{sol} of 18.8%, and likewise, kept an excellent T_{lum} of 54.3%, which was preferred to most VO_2 nano-composite films and multilayered VO_2 films. Fig. 5(c) shows the spectra between transmittance and ZnO/VO_2. They observed that the reflectance of various samples was reduced by enhancing the content of ZnO NPs. This indicated that ZnO NPs separated uniformly in the VO_2–ZnO composite layer that decreased the reflectance of VO_2 films similar to the anti-reflection coatings (ARCs), and increased both T_{lum} and ΔT_{sol} concurrently. Further, instead of metal oxides, the polymer material has been tried to explore the thermochromic properties of the hybrid of VO_2. Z. Qu and coworkers prepared VO_2 nanoparticles that were embedded on cross-linked polymethyl methacrylate (PMMA) chains as seen in Fig. 5(d).[102] The enhanced luminous transmittance of light along with a better solar transmittance was obtained by this synthesized VO_2 NP. They obtained a luminous transmittance of about 50%, a solar modulation ability of about 17.1%, and a haze of about 11% *via* the cross-linked PMMA-VO_2 film. The graphical results represented that the luminous transmittance was decreased at a high temperature of 90 °C, while it increased largely at 25 °C. The values obtained from the graph were ~50% luminous transmittance and approximately equal to 17.1% solar modulation ability. The graph represented value is decreasing by increasing the wavelength of light. It can be further reduced by decreasing the size of the VO_2 NP. The graph provides us with an average value of haze equal to 11% that was in the luminous range. In Fig. 5(e) a comparison graph between solar modulation and time (h) shows the transmittance and durability of VO_2. To check the durability of PMMA-VO_2, the following conditions were sustained: low temperature of 25 °C (insulating phase), high temperature of 90 °C (metallic phase), and relative humidity of ~95%, and an aging chamber for aging

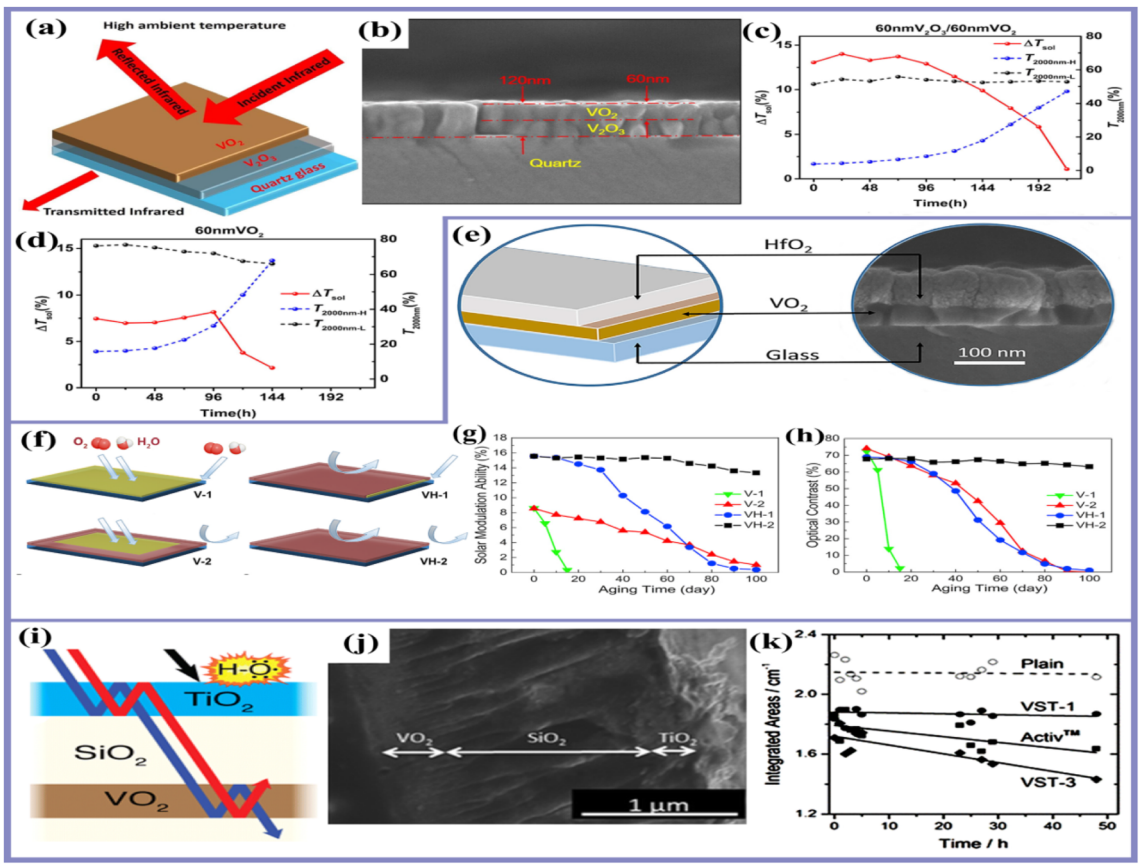

Fig. 6 (a) Experimental flow chart for the synthesis of the V_2O_3/VO_2 bi-layer structure and (b) SEM images of the V_2O_3/VO_2 bi-layer structure. (c) Transmittance spectra of 60 nm VO_2 at different times in hours. (d) 60 nm V_2O_3/VO_2 at different times in hours. Reproduced with permission[107] Copyright © 2018, Elsevier. (e and f) Flow chart for the whole process of VO_2/HfO_2 thin films by using the sputtering method and SEM images. (g) Graph of solar modulation ability *versus* aging time. (h) Durability of the fabricated films with the graph between optical contrast and aging time (days). Reproduced with permission[108] Copyright © 2019, Elsevier. (i) Preparation of VO_2/SiO_2/TiO_2 thin layers. (j) TEM images of VO_2/SiO_2/TiO_2 thin layers. (k) Durability graph of the VO_2/SiO_2/TiO_2 thin film. Reproduced with permission[109] Copyright © 2016, American Chemical Society.

tests had a constant temperature of 60 °C. The results exhibited that the cross-connected PMMA-VO_2 film had a longer life than the non-cross-connected PMMA-vanadium dioxide film having a large molecular weight. So, this research shows a greater enhancement in the durability of VO_2 for smart window applications. The PMMA-VO_2 film played a greater role in weather-resistance; it minimized the cooling demands at high temperatures and enhanced the warm comfort in cooling climates. The fabricated VO_2 nanoparticle enhanced the luminous transmittance (~50%), solar modulation ability (~17.1%), haze (~11%), and lifespan as compared to simple VO_2 nanoparticles. These results of nanoparticle-based thermochromic films exhibit a robust durability.

2.3.2 VO_2-based thin film structures *via* the layer-by-layer strategy. The thin film is prepared *via* spin coating method, the matrix materials are entangled with active VO_2-nanoparticles. The effects of coating materials in thin-film structural modification are clearly seen by the sputtering method based thin film.[103–106] Like other physical vapor deposition techniques, ion beam sputtering provides advantages such as deposition rate, uniformity, composition, thickness control, adhesion, and material properties. However, ion beam sputtering offers additional sputter deposition features, which include a wide range of materials with indifference to target thickness or properties, precision deposition stops, clean and low pressure processing (<0.5 mTorr), and reactive deposition not susceptible to high energy arcs due to cathode target poisoning. In the ion beam deposition process, there is no plasma between the substrate and the target as one would find with magnetron sputtering. This means that the ion beam deposition technique can be used for deposition on sensitive materials and reduces the likelihood that the final product will contain gas molecules.

To elaborate the effects of thin film coating on the durability of VO_2 in smart window applications, thin films have been tried by altering the various coating materials. For example, additionally, S. Long and coworkers prepared a high-quality V_2O_3/VO_2 bi-layer structure.[107] To enhance the crystallinity of the VO_2 thin film, the bottom layer of V_2O_3 behaved as the buffer layer as seen in Fig. 6(a). The fabricated film was used to increase the luminous transmittance, solar modulation ability, and durability of the vanadium dioxide film. They displayed the durability of the fabricated film; the film was kept at 60 °C and had a humidity of 90%. The SEM images clearly show the presence of V_2O_3 and VO_2 as can be seen in Fig. 6(b). The simple VO_2 film was damaged after 72 hours and completely depleted after 144 h (~6 days) as compared to this V_2O_3/VO_2 thin film which retained itself at 144 h (~6 days) (Fig. 6(c)); the same is the case for solar modulation ability ΔT_{sol}. Finally, Fig. 6(d) describes that the fabricated films (V_2O_3/VO_2) had maintained the luminous intensity for a long duration and also provided good durability and solar modulation ability of 13.2%, which was increased by 76%. T. Chang and coworkers designed VO_2/HfO_2 thin films *via* the sputtering method, the SEM images of which can be seen in Fig. 6(e) and (f).[108] The fabricated film had an encapsulation structure that has more stability than a single vanadium film. The thermochromic properties were enhanced by using HfO_2 with VO_2. This increased luminous intensity and solar modulation ability. The fabricated film VO_2/HfO_2 protected the VO_2 layer from weather changes and provided comprehensive protection. It also increased the service life of VO_2 and the stability of the VO_2 film. A comparison of the simple VO_2 film and VO_2/HfO_2 showed that the VO_2/HfO_2 layer has high luminous transmittance, T_{lum} = 55.8% (at low temperature) and T_{lum} 43.6% (at high temperature), and high solar modulation ΔT_{sol} = 15.9%. So, as a result, we can see a total of 80.1% improved properties with VO_2/HfO_2. For testing the durability of the fabricated films, the sample was placed in a harsh environment at a temperature of 60 °C and humidity of 90% as shown in Fig. 6(g). Moreover, Fig. 6(h) represents the graph of solar modulation ability *versus* aging time; it is clear that the simple VO_2 film lost its thermochromic properties, and showed enhanced properties that last for a few time span when combined with silicon weatherproof sealant. The sample showed greater stability that lasted for 100 days, proving that the product was more efficient than simple VO_2. The guaranteed life for their fabricated film was about 16 years as indicated from the graph that satisfied the demand for practical applications. The VO_2 converts into V_2O_5 oxide when heated at high temperature (annealing temperature) but the use of HfO_2 as an antireflection agent protects it from the formation of oxides. So, by introducing the VO_2/HfO_2 film they got large luminous intensity ranging from 55.8% and sun modulation of 15.9%, and the film was more stable than it could be in the actual form for 16 years.

Further, the double layer of the thin film consisting of different materials on VO_2 has also been investigated in terms of thermochromic properties. For example, M. J. Powell and coworkers prepared the VO_2/SiO_2/TiO_2 thin layers.[109] In the structure, the VO_2 layer with SiO_2 was over layered by TiO_2 as shown in Fig. 6(i). Furthermore, Fig. 6(j) depicts the TEM of VO_2/SiO_2/TiO_2 thin layers. The results indicated that by inserting these layers the transmission of visible light dramatically increased and the solar modulation of the material doubled. The scotch tape test was performed, which justified that the single VO_2 layer could be easily delaminated but the multilayer VO_2/silicon di-oxide/TiO_2 demonstrated high adherence to glass substrates. Moreover, the deposited films were irradiated with broad band light sources. The values of transmittance were taken between the regions with direct contact between air with TiO_2 and region of SiO_2 (glass) in direct contact with the bottom layer of VO_2. The modern window metrics T_{lum} and ΔT_{sol} were measured for every layer of VO_2. The results with an incoherent layer of SiO_2 exhibited the lesser resonant peaks. For the sample of VST-1, the smart window was demonstrated by a model of transfer matrix showing the thickness of VO_2, which enhanced and reached the value of 50 nm. This suggests that the VO_2 film has a low density. The graph in Fig. 6(k) represents the durability of the VO_2/SiO_2/TiO_2 thin film. Their new manufactured thin layer coating on VO_2 resulted from an increase in solar modulation and visible light transmittance. SiO_2/TiO_2 layers on VO_2 enhanced the mechanical properties of the smart windows. The solar modulation value acquired in the said experiment was 15.29%, which is the best value for VO_2. This result about

environmental durability, which has rarely been considered, is also so vital for practical application.

The bilayer coating strategy has delivered the most prominent results for fixing the oxidation problems of VO_2 against humid environments.[110–115] X. Zhou and coworkers developed a new strategy to fabricate a VO_2 coating with long-term stability, low critical temperature (t_c), significantly enhanced thermochromic performance and low fabrication cost by using the room temperature PVD deposition of amorphous VO_x.[116] It is followed by rapid thermal annealing (RTA) in air for less than 10 min. This process renders a fascinating VO_2 nanocomposite structure within a V_2O_5 and V_3O_7 matrix encapsulated in a dense amorphous V_2O_5 overcoat, which is impossible to obtain by the usual PVD approach. Moreover, the sample could be exposed to the normal atmosphere for more than 2 years and remain intact. Accelerated results suggested that the sample can maintain the good thermochromic performance of T_{lum} (42.2%) and ΔT_{sol} (14.6%) after 23 years. H. Zhou and coworkers prepared a multifunctional bilayer VO_2/ZnO (VZ) film to improve the thermochromic properties of the VO_2 film.[117] The ZnO thin film acts as an anti-reflection layer to protect the film from corrosion. Furthermore, transmittance spectra shows a comparison graph between concentrations and immersion durations for simple VO_2 and VO_2/ZnO films. In comparison to the simple VO_2 film, the VO_2/ZnO film depicted a greater anti-reflection property. The ZnO behaves differently in weather conditions; in cold days it absorbs light to warm up the room, while in hot days it is reflective to IR light but transparent to visible light, displaying a luminous transmittance of 50.3% enhanced from 40.6% and solar modulation ability of 11.2% enhanced from 7.7%. J. Zhang and coworkers prepared a mesoporous silicon dioxide/VO_2 double layer system.[118] The film was fabricated to increase the refractive index from 1.243 to 1.354. The extinction coefficient K_v and refractive index n_v were calculated by fitting the results which were obtained by the Drude Lorentz method. The graph showed that a refractive index lesser than 2 was obtained by the said fabrication method. The transmission of visible light was promoted by lowering the refractive index. The near infrared ray (NIR) switching and high visible transmittance were obtained by the fabricated film that demonstrated the existence of monoclinic VO_2. The NIR switching ability was obtained to be 32.1% at 2000 nm, and the transmittance of visible light ($T_{vis,\ L}$) was obtained to be 69.8% in addition to a solar transmittance (ΔT_{sol}) of 12.6%. The graph depicted the high crystallinity, which assured the good quality of synthesized VO_2. The visible transmittance was 80% by using a refractive index of 1.299 that of SiO_2. This work would be a milestone in energy-saving smart windows of VO_2-based thermochromic coatings. S. Loquai and coworkers deposited a VO_2 thin film to study the environmental stability.[119] The SEM images exhibited an increase in surface roughness due to identical $\Delta T_{2500\ nm}$ behavior, and both radio-frequency magnetron sputtering (RFMS) and high-power impulse magnetron sputtering (HiPIMS) behaved almost similarly in critical temperature (T_c) performance as seen in Fig. 7(a) and (b). Moreover, a graph between transmittance and time (h)

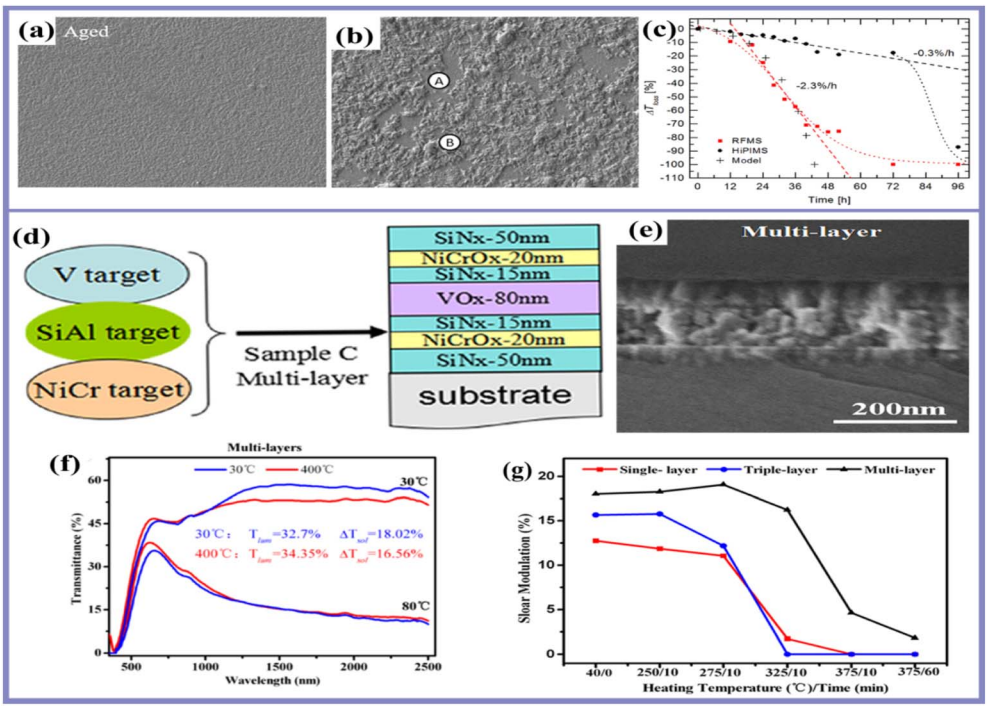

Fig. 7 (a and b) SEM images of the deposited VO_2 thin film and comparison study between RFMS and HiPIMS. (c) Transmittance spectra of the thin film. Reproduced with permission[119] Copyright © 2016, Elsevier. (d) Preparation of films such as single layer as G/VO_x, triple-layer as G/SiN_x/VO_x/SiN_x, and multi-layer. (e) SEM images of the as synthesized films. (f) Optical transmittance spectra of the films. (g) Solar modulation of the triple layer. Reproduced with permission[125] Copyright © 2017, Elsevier.

depicts that the as synthesized materials have better thermochromic characteristics, which can be easily observed in Fig. 7(c). But visible transmission of HiPIMS was lower due to its higher refractive index and high extinction coefficient of the film, which illustrates the loss per hour for both RFMS and HiPIMS film. The RFMS film had a 2.3% loss per hour, while HiPIMS acquired a 0.3% loss per hour, which exposed that HiPIMS deposition was better than RFMS deposition. The research says that HIPIMS deposition is significantly better for environmental stability as compared with RFMS due to its larger grain size, high density, and lower hydrogen intake. As compared to RFMS the HiPIMS film deposition has approximately three times longer lifespan. The suggested deposition method with the help of achieved results was considered attractive *via* HiPIMS.

Further, for making a thin film, the multilayer strategy has also been investigated by choosing various materials (TiO_2, NiCr, SiN, *etc.*) with VO_2 and their thermochromic properties have been explored against weather resistance.[120–124] For example, Y. Zhan and coworkers designed three VO_x-based thin films having different layers, *i.e.*, single, triple and multilayered.[125] The distributions of films were prepared, such as single layer as G/VO_x, triple-layer as G/SiN_x/VO_x/SiN_x, and multilayer as G/SiN_x/$NiCrO_x$/SiN_x/VO_x/SiN_x/$NiCrO_x$/SiN_x as observed in Fig. 7(d). The cross-sectional SEM images reveal the stress, grain size, and other defects present in the fabricated film. Fig. 7(e) shows the surface roughness of the multilayer. It is verified that the triple-layer and multilayer have a higher density of grain boundaries that is good for transmission from the semiconductor to metal. The optical transmittance of the three fabricated layers before and after thermal treatment at a low temperature of 30 °C and a high temperature of 60 °C was discussed. The luminous transmittance of all samples increased with increasing temperature as seen in Fig. 7(f) but above 325 °C the switching decreased greatly due to another phase in films. The vanadium pentoxide (V_2O_5) formed at 375 °C due to which thermochromic properties vanished at that temperature. In Fig. 7(g), a good optical switching in the triple layer was observed at 275 °C and it became zero level above 325 °C due to formation of VO_2. Moreover, the thermal stability of the multi-layer thin film was excellent below 325 °C and came to zero at 375 °C, and the T_{lum} remained stable below 325 °C. The luminous transmittance got stable at a high temperature of 80 °C with a numerical value of 34.35% and a solar modulation of 16.56% also stabled as discussed in Fig. 7(f). As defining the results of this film, we can say that this fabricated film enhances the thermochromic property of VO_2. As VO_2 was reduced to V_2O_5 after being placed in air, this imperfection in VO_2 was removed by making multilayers from this method. Hence, multilayers provided us a T_{lum} value of 34.35% and solar modulation ability of 18.02%. The above mentioned nanomaterials represent a promising candidate for energy-efficient thermochromic smart windows for enhancing weather resistance properties.

2.3.3 VO_2-based thin film structures *via* a sandwich-strategy. The major advantages of sandwich composites over conventional materials are that sandwich composites (1) have a low overall density, a high strength-to-weight ratio, and a high stiffness-to-weight ratio; (2) are capable of providing good thermal and acoustic insulation; and (3) have uniform energy absorption capacity. To avoid contamination of VO_2 in hybrids from environment and substrate, the sandwich-like structural modification is played an excellent role in stabilizing the hybrid against harsh environments. Sandwich-like structural adaptions have been tried by using different materials in the thin film strategy.[126–135] For example, S. Long and coworkers designed SiN_x/VO_2(SV), VO_2/SiN_x (VS), and SiN_x/VO_2/SiN_x (SVS) multilayers as shown in Fig. 8(a).[136] The fabricated film played a better role in the advancement of solar modulation ability and luminous transmittance. The TEM images show the different size of thin layers as seen in Fig. 8(b). An experimental test was performed to observe the retention of luminous transmittance and solar modulation ability of the VO_2 film in comparison with the fabricated SVS thin film. The luminous transmittance $T_{2500\ nm}$ started to decrease after 1600 cycles for the simple VO_2 film and retained only 20.1%. But in the case of the SVS film after passing 10 000 cycles, the luminous intensity decreased very slowly such that it retained 98.3% of its initial value. Moreover, it retained 88.1% of its initial value after passing 27 000 cycles, showing the best performance of the fabricated film. The experimental results revealed that the lifespan of the SVS film would be approximately 27 years, which was more than that of the simple VO_2, which was just 4 years. To check out the durability of the SVS film, the film was kept at 60 °C and humidity of 90% as observed in Fig. 8(c). The simple VO_2 film was damaged after 144 hours and completely depleted after 192 h (~8 days). As compared to this, the SVS thin-film caught depletion after 480 h and completely depleted after 600 h (~25 days) as shown in Fig. 8(d). This demonstrated that the fabricated film sustained 3 times more than VO_2 films; solar modulation ability had a similar tendency, which depicted a luminous transmittance of 39.1% and solar modulation ability of 14.2% for SiN_x/VO_2/SiN_x films. The SVS structure has more lifespan and durability as compared to a single VO_2 layer. Further, by varying the materials in the layers of a sandwich structure, the hybrids were also investigated; T. Chang and coworkers arranged a sandwiched structure of Cr_2O_3/VO_2/SiO_2 (CVS) on a glass substrate as observed in Fig. 8(e).[137] The bottom layer of Cr_2O_3 had improved the crystallinity of VO_2 and increased the luminous transmittance of the structure. The upper layer of SiO_2 acted as an anti-reflectant to light and also increased the environmental stability by providing a self-cleaning layer. The results of the as-prepared thin film have enhanced the durability of simple VO_2 as well as the luminous intensity and solar transmittance. The solar modulation ability of the fabricated CVS thin film is 16.1%, which is more efficient, and the obtained luminous transmittance is 54%. The durability graphs of simple VO_2, Cr_2O_3/VO_2, and Cr_2O_3/VO_2/SiO_2 exhibited the credibility of fabricated CVS thin films over other ones. The graph presented that the CVS film retained its thermochromic properties after thousands of hours, while the simple VO_2 had left over after a few hours only. The sample was kept at a high temperature of 60 °C and relative humidity of 90% for many hours. To endure the environmental damages, the VO_2 has to undergo phase transition between metallic and

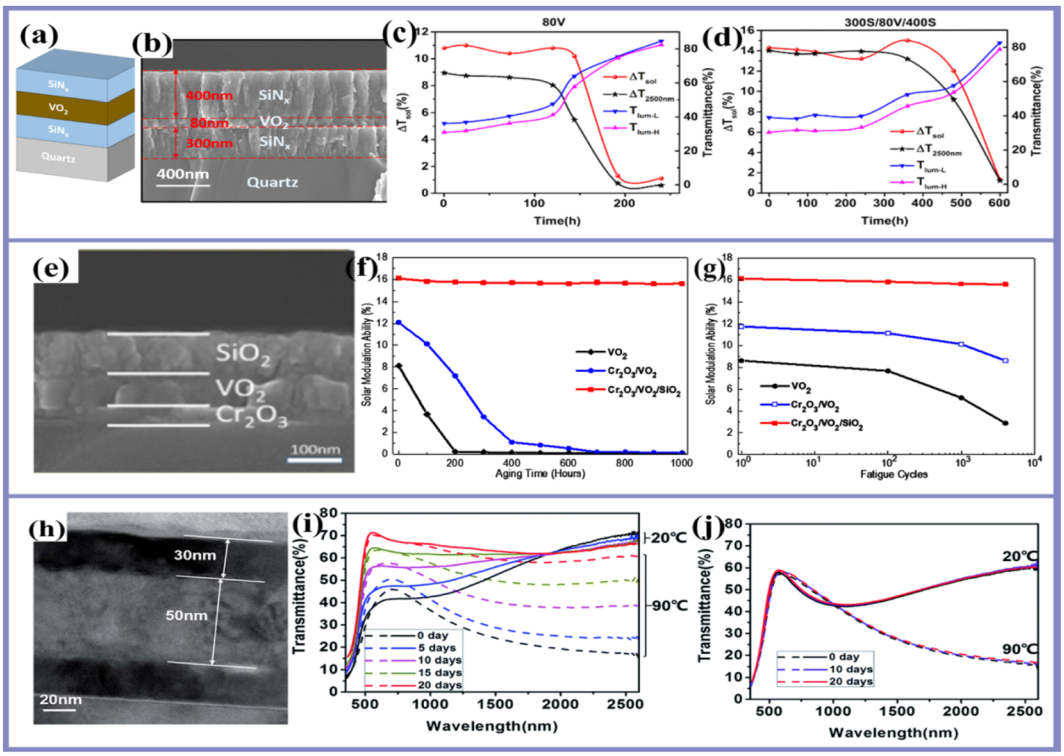

Fig. 8 (a) Preparation of SiN_x/VO_2(SV), VO_2/SiN_x (VS), and $SiN_x/VO_2/SiN_x$ (SVS) multilayers by using the reactive magnetron sputtering method. (b) Field Emission Scanning Electron Microscopy (FE-SEM) of the multilayers. (c) Durability graph of the SVS film at 60 °C and humidity of 90%. (d) Comparison graph of the aging test. Reproduced with permission[136] Copyright © 2018, Elsevier. (e) Preparation of the sandwiched structure of $Cr_2O_3/VO_2/SiO_2$ (CVS) on a glass substrate by using the magnetron sputtering process and SEM images. (f) Fatigue test of simple VO_2 and structures. (g) Comparison graph of single VO_2 layer and SVS layers. Reproduced with permission[137] Copyright © 2017, Elsevier. (h) SEM image of the as prepared sandwiched structure of $WO_3/VO_2/WO_3$ on VO_2 by using the medium frequency reactive magnetron sputtering technique (MFRMST) and HRTEM images. (i) Durability graph of the prepared layer under different temperature and humidity conditions. (j) Aging test of the VO_2 sample and thin-film $WO_3/VO_2/WO_3$. Reproduced with permission[138] Copyright © 2016, The Royal Society of Chemistry.

semiconducting states once a day as can be seen in Fig. 7(f). The results of the fatigue test for different cycles showed that the single VO_2 layer deteriorated after 4000 cycles and only 33% thermochromic properties were sustained, while the CVS thin film had constant thermochromic properties after 4000 cycles as observed in Fig. 7(g). It was clear that we can get a more reliable and durable product by using the above mentioned method. This thin film has two non-reflecting agents at both ends that enhance the solar modulation ability of the VO_2, as well as luminous intensity. By using this film they achieved a luminous intensity of 54% and solar modulation ability of about 16.1%, enhancing the thermochromic properties of VO_2. Furthermore, both layers of the sandwich structure were replaced by metals and thermochromic properties were explored. S. Long and coworkers prepared a sandwiched structure of $WO_3/VO_2/WO_3$ that was deposited on VO_2 to improve the transmittance of visible light and durability.[138] The TEM image depicts that a 50 nm layer of VO_2 was sandwiched between 30 nm layers of WO_3 as clearly observed in Fig. 8(h), where WO_3 acted as an anti-reflection (AR) agent at both the top and bottom sides. The sandwiched structure of VO_2 with WO_3 has many useful effects on the smart window. The luminescence of light, as well as transmittance for infrared light, was enhanced by using this thin layer. The luminescence (T_{lum}) was dramatically increased by a factor of 49% (from 37.2% to 55.4%), and also the hysteresis loop became sharper as the double layer of WO_3 enhanced the luminous transmittance (T_{lum}) and it acted as a better-guarding layer for the thermo chromic property of VO_2. The transition temperature for the single VO_2 layer is 54.5 °C, which was reduced to 52 °C by inserting WO_3 layers ($WO_3/VO_2/WO_3$). Fig. 8(i) represents the durability of the prepared layer under different temperature and humidity conditions. The VO_2 sample and thin-film $WO_3/VO_2/WO_3$ have remained in 20 °C temperature and 90% humidity for 5, 10, 15, and 20 days. The results displayed that the thermo chromic property of a single layer of VO_2 vanished after 20 days. When VO_2 was coated with WO_3 on the top and bottom side, the durability enhanced such that it remained unaffected after 20 days as shown in Fig. 8(j). So the obtained results have an excellent proof for the preparation of thin films such as $WO_3/VO_2/WO_3$ which had better results than the single VO_2, and enhanced the luminous transmittance of light with increasing the durability for smart window application. The results about VO_2-based thin film structures *via* the sandwich-strategy showed the best performance for weather resistance in smart windows.

3. Summery/future outlook

VO_2 depicts great potential as the next-generation smart glazing for architecture owing to its automatic thermochromic effect depending on ecological temperatures. The thermochromic characteristics of VO_2 smart windows have been improved previously with tremendous efforts. However, the fundamental obstacle in the practical application of VO_2 in smart windows is the poor stability of VO_2 against an environment containing air moisture and other active elements. In order to establish carbon-neutral future, it is thus necessary to reduce the consumption of energy from non-renewable sources and decrease the energy demand through energy saving, environmentally friendly technologies. In this perspective, thermochromic smart windows, which can regulate the flow of energy during the day and provide lighting during the night, might reduce the demand for separate lighting systems and reduce the demand for energy for cooling. To overcome the effects emerging from unstable VO_2 in an open environment, some attempts have been made through different strategies in our review. This review investigates the challenges and opportunities of VO_2-based smart glazing that may be beneficial in accelerating the realization of real-world applications. This systematically summarises the recent progress in weather resistance that is currently in the stage of research and examines the quantitative parameters of smart window devices. Currently existing and still developing thermochromic technologies open up a very wide range of possibilities for their use in construction. This is the reason why broad research is necessary, and hopefully it will finally be able to identify technologies that have the potential of scaling, which seems to be one of the most important challenges of the weather resistance technology. Even though earlier research has overcome many of the other issues that impede practical applications, much development is still required before the technology becomes fully incorporated into our lives. The following are some suggestions for further study on VO_2 based energy-efficient windows. Firstly, there are many different hues for colors, and colors can change throughout time. To obtain an aesthetic appeal, VO_2 based coatings on smart windows must be changed from their unattractive brown-yellowish color. VO_2 can produce a variety of colors and temperature-responsive color shifts when combined with other thermochromic or functional chemicals. More focus is needed to increase the longevity of VO_2 hybrids, which could involve structural changes made with other types of materials. Secondly, material modification is an effective tool for creating new useful materials. Developing VO_2 based film smart windows could be possible by combining VO_2 films with additional functional materials that can provide new functions and/or enhance VO_2 based films. Such kinds of functional materials ought to be used to improve the stability of VO hybrids for applications in smart windows. Lastly, the final product under consideration must be produced in large quantities at low cost and with high quality. The future development of thermochromic smart coatings will depend on the creation of straightforward but effective scaling up procedures for synthesis and film deposition. This capability necessitates proper changes in order to integrate various technologies into glass manufacturing lines effectively.

Author contributions

Muhammad Khuram Shahzad and Rana Zafar Abbas Manj have equal contributions and wrote the whole review manuscript including idea, Ghulam Abbas, Rashid Ali Laghari, Syed Sohail Akhtar, Muhammad Aslam Khan and Muhammad Bilal Tahir prepared all the figures and reviewed the manuscript, and Sami Znaidia and Meshal Alzaid revised the reviewer comments.

Conflicts of interest

No conflict of interest.

Acknowledgements

The author (Sami Znaidia) extends his appreciation to the Deanship of Scientific Research at King Khalid University for funding this work through Large Groups Project under grant number RGP.2/166/43.

References

1 C. G. Granqvist, S. Green, G. A. Niklasson, N. R. Mlyuka, S. von Kræmer and P. Georén, *Thin Solid Films*, 2010, **518**, 3046–3053.
2 C. G. Granqvist, *Thin Solid Films*, 2016, **614**, 90–96.
3 C. G. Granqvist, *Mater. Today: Proc.*, 2016, **3**, S2–S11.
4 G. Wei, X. Fan, Y. Xiong, C. Lv, S. Li and X. Lin, *Appl. Phys. Express*, 2022, **15**(4), 043002.
5 C. G. Granqvist, P. C. Lansåker, N. R. Mlyuka, G. A. Niklasson and E. Avendaño, *Sol. Energy Mater. Sol. Cells*, 2009, **93**, 2032–2039.
6 S. K. Deb, *Sol. Energy Mater. Sol. Cells*, 2008, **92**, 245–258.
7 C. G. Granqvist, İ. Bayrak Pehlivan, Y. X. Ji, S. Y. Li and G. A. Niklasson, *Thin Solid Films*, 2014, **559**, 2–8.
8 J. Wang, L. Zhang, L. Yu, Z. Jiao, H. Xie, X. W. Lou and X. Wei Sun, *Nat. Commun.*, 2014, **5**, 4921.
9 F. Zhang, X. Zhao, R. Li, S. He, X. Tan, J. Zhu and R. Ang, *J. Mater. Chem. A*, 2022, DOI: **10.1039/D2TA06980F**.
10 X. Fan, G. Wei, X. Lin, X. Wang, Z. Si, X. Zhang and W. Zhao, *Matter*, 2020, **2**(6), 1582–1590.
11 C. G. Granqvist, *Sol. Energy Mater. Sol. Cells*, 2012, **99**, 1–13.
12 J. Zheng, S. Bao and P. Jin, *Nano Energy*, 2015, **11**, 136–145.
13 S. M. Babulanam, T. S. Eriksson, G. A. Niklasson and C. G. Granqvist, *Sol. Energy Mater.*, 1987, **16**, 347–363.
14 S. Wang, T. Jiang, Y. Meng, R. Yang, G. Tan and Y. Long, *Science*, 2021, **374**(6574), 1501–1504.
15 Y. Ke, Y. Li, L. Wu, S. Wang, R. Yang, J. Yin, G. Tan and Yi Long, *ACS Energy Lett.*, 2022, **7**(5), 1758–1763.
16 S. Wang, Y. Zhou, T. Jiang, R. Yang, G. Tan and Y. Long, *Nano Energy*, 2021, **89**, 106440.
17 R. Binions, G. Hyett, C. Piccirillo and I. P. Parkin, *J. Mater. Chem.*, 2007, **17**, 4652–4660.

18 P. Evans, M. E. Pemble, D. W. Sheel and H. M. Yates, *J. Photochem. Photobiol., A*, 2007, **189**, 387–397.
19 J. Shi, S. Zhou, B. You and L. Wu, *Sol. Energy Mater. Sol. Cells*, 2007, **91**, 1856–1862.
20 S. Li, C. Lv, X. Lin, G. Wei, Y. Xiong, W. Yang and W. Zhao, *Appl. Phys. Lett.*, 2021, **119**(12), 122401.
21 M. La, H. Zhou, N. Li, Y. Xin, R. Sha, S. Bao and P. Jin, *Appl. Surf. Sci.*, 2017, **403**, 23–28.
22 W. U. Rehman, H. Wang, R. Z. A. Manj, W. Luo and J. Yang, *Small*, 2021, **17**, 1904508.
23 M. K. Shahzad, Y. Zhang, L. Cui, L. Liu, M. K. Butt and H. Li, *RSC Adv.*, 2018, **8**, 19362–19368.
24 W.-L. Jang, Y.-M. Lu, C.-L. Chen, Y.-R. Lu, C.-L. Dong, P.-H. Hsieh, W.-S. Hwang, J.-L. Chen, J.-M. Chen, T.-S. Chan, J.-F. Lee and W.-C. Chou, *Phys. Chem. Chem. Phys.*, 2014, **16**, 4699–4708.
25 C. Guo, Z. Zhang, Y. Wu, Y. Wang, G. Ma, J. Shi and Y. Zhao, *Supercond. Sci. Technol.*, 2022, **35**, 075014.
26 V. Wittwer, M. Datz, J. Ell, A. Georg, W. Graf and G. Walze, *Sol. Energy Mater. Sol. Cells*, 2004, **84**, 305–314.
27 N. Li, Y. Li, G. Sun, Y. Ma, T. Chang, S. Ji, H. Yao, X. Cao, S. Bao and P. Jin, *Chem.–Asian J.*, 2017, **12**, 1709–1714.
28 N. Li, Y. Li, Y. Zhou, W. Li, S. Ji, H. Yao, X. Cao and P. Jin, *Sol. Energy Mater. Sol. Cells*, 2017, **160**, 116–125.
29 N. Li, Y. Li, W. Li, S. Ji and P. Jin, *J. Phys. Chem. C*, 2016, **120**, 3341–3349.
30 Z. Chen, Y. Gao, L. Kang, J. Du, Z. Zhang, H. Luo, H. Miao and G. Tan, *Sol. Energy Mater. Sol. Cells*, 2011, **95**, 2677–2684.
31 M. K. Dietrich, F. Kuhl, A. Polity and P. J. Klar, *Appl. Phys. Lett.*, 2017, **110**, 141907.
32 J. Schläefer, C. Sol, T. Li, D. Malarde, M. Portnoi, T. J. Macdonald, S. K. Laney, M. J. Powell, I. Top, I. P. Parkin and I. Papakonstantinou, *Sol. Energy Mater. Sol. Cells*, 2019, **200**, 109944.
33 S. Saitzek, F. Guinneton, L. Sauques, K. Aguir and J.-R. Gavarri, *Opt. Mater.*, 2007, **30**, 407–415.
34 H. Zhou, X. Cao, M. Jiang, S. Bao and P. Jin, *Laser Photonics Rev.*, 2014, **8**, 617–625.
35 F. J. Morin, *Phys. Rev. Lett.*, 1959, **3**, 34–36.
36 Z. Zhang, Y. Gao, H. Luo, L. Kang, Z. Chen, J. Du, M. Kanehira, Y. Zhang and Z. L. Wang, *Energy Environ. Sci.*, 2011, **4**, 4290–4297.
37 N. Li, Y. Li, G. Sun, Y. Zhou, S. Ji, H. Yao, X. Cao, S. Bao and P. Jin, *Nanoscale*, 2017, **9**, 8298–8304.
38 M. Tazawa, H. Asada, G. Xu, P. Jin and K. Yoshimura, *MRS Online Proc. Libr.*, 2004, **785**, 105.
39 M. Li, S. Magdassi, Y. Gao and Y. Long, *Small*, 2017, **13**, 1701147.
40 M. E. A. Warwick and R. Binions, *J. Mater. Chem. A*, 2014, **2**, 3275–3292.
41 Y. Gao, H. Luo, Z. Zhang, L. Kang, Z. Chen, J. Du, M. Kanehira and C. Cao, *Nano Energy*, 2012, **1**, 221–246.
42 Y. Gao, S. Wang, L. Kang, Z. Chen, J. Du, X. Liu, H. Luo and M. Kanehira, *Energy Environ. Sci.*, 2012, **5**, 8234–8237.
43 G. Sun, H. Zhou, X. Cao, R. Li, M. Tazawa, M. Okada and P. Jin, *ACS Appl. Mater. Interfaces*, 2016, **8**, 7054–7059.
44 G. Sun, X. Cao, X. Li, S. Bao, N. Li, M. Liang, A. Gloter, H. Gu and P. Jin, *Sol. Energy Mater. Sol. Cells*, 2017, **161**, 70–76.
45 G. Sun, X. Cao, H. Zhou, S. Bao and P. Jin, *Sol. Energy Mater. Sol. Cells*, 2017, **159**, 553–559.
46 S. Li, Y. Li, M. Jiang, S. Ji, H. Luo, Y. Gao and P. Jin, *ACS Appl. Mater. Interfaces*, 2013, **5**, 6453–6457.
47 Y. Li, S. Ji, Y. Gao, H. Luo, S. Li, M. Jiang, Y. Zhou, R. Li, B. Wang and P. Jin, *CrystEngComm*, 2013, **15**, 8330–8336.
48 J. Zhu, A. Huang, H. Ma, Y. Chen, S. Zhang, S. Ji, S. Bao and P. Jin, *New J. Chem.*, 2017, **41**, 830–835.
49 Y. Ke, X. Wen, D. Zhao, R. Che, Q. Xiong and Y. Long, *ACS Nano*, 2017, **11**, 7542–7551.
50 Y. Li, S. Ji, Y. Gao, H. Luo and P. Jin, *ACS Appl. Mater. Interfaces*, 2013, **5**, 6603–6614.
51 H. Liu, D. Wan, A. Ishaq, L. Chen, B. Guo, S. Shi, H. Luo and Y. Gao, *ACS Appl. Mater. Interfaces*, 2016, **8**, 7884–7890.
52 S.-D. Lan, C.-C. Cheng, C.-H. Huang and J.-K. Chen, *Appl. Surf. Sci.*, 2015, **357**, 2069–2076.
53 M. Li, H. Wu, L. Zhong, H. Wang, Y. Luo and G. Li, *J. Mater. Chem. C*, 2016, **4**, 1579–1583.
54 J. Wan, Q. Ren, N. Wu and Y. Gao, *J. Alloys Compd.*, 2016, **662**, 621–627.
55 Y. Li, P. Jiang, W. Xiang, F. Ran and W. Cao, *J. Colloid Interface Sci.*, 2016, **462**, 42–47.
56 J. Zhang, T. Wang, W. Xu, X. Yang, X. Zuo, W. Cheng and C. Zhou, *Nanotechnology*, 2021, **32**, 225402.
57 Y. Luo, M. Li, K. Li, C. Xu, S. Xu and G. Li, *Sol. Energy Mater. Sol. Cells*, 2019, **191**, 258–265.
58 H. Ji, D. Liu, C. Zhang and H. Cheng, *Sol. Energy Mater. Sol. Cells*, 2018, **176**, 1–8.
59 D. Wang, D. Guo, Z. Zhao, C. Ling, J. Li, S. Hong, Y. Zhao and H. Jin, *Sol. Energy Mater. Sol. Cells*, 2019, **200**, 110031.
60 L. Xuanming, *RSC Adv.*, 2016, **6**, 47249–47257.
61 M. Xygkis, E. Gagaoudakis, L. Zouridi, O. Markaki, E. Aperathitis, K. Chrissopoulou, G. Kiriakidis and V. Binas, *Coatings*, 2019, **9**(3), 163.
62 M. Saini, B. S. Dehiya and A. Umar, *Ceram. Int.*, 2020, **46**, 986–995.
63 S. Y. Li, G. A. Niklasson and C. G. Granqvist, *J. Appl. Phys.*, 2011, **109**, 113515.
64 Z. Wen, Y. Ke, C. Feng, S. Fang, M. Sun, X. Liu and Y. Long, *Adv. Mater. Interfaces*, 2021, **8**, 2001606.
65 Y. Chen, J. Zhu, H. Ma, L. Chen, R. Li and P. Jin, *Sol. Energy Mater. Sol. Cells*, 2019, **196**, 124–130.
66 Y. Chen, X. Zeng, J. Zhu, R. Li, H. Yao, X. Cao, S. Ji and P. Jin, *ACS Appl. Mater. Interfaces*, 2017, **9**, 27784–27791.
67 S. Zhao, Y. Tao, Y. Chen, Y. Zhou, R. Li, L. Xie, A. Huang, P. Jin and S. Ji, *ACS Appl. Mater. Interfaces*, 2019, **11**, 10254–10261.
68 Z. Qu, L. Yao, J. Li, J. He, J. Mi, S. Ma, S. Tang and L. Feng, *ACS Appl. Mater. Interfaces*, 2019, **11**, 15960–15968.
69 K. Tong, R. Li, J. Zhu, H. Yao, H. Zhou, X. Zeng, S. Ji and P. Jin, *Ceram. Int.*, 2017, **43**, 4055–4061.
70 Z. Fang, S. Tian, B. Li, Q. Liu, B. Liu, X. Zhao and G. Sankar, *Appl. Surf. Sci.*, 2021, **540**, 148414.
71 M. Salamati, G. Kamyabjou, M. Mohamadi, K. Taghizade and E. Kowsari, *Constr. Build. Mater.*, 2019, **218**, 477–482.

72 M. K. Shahzad, U. Farooq, A. Raza, G. Abbas, M. Ikram and Y. Zhang, *RSC Adv.*, 2021, **11**, 36569–36576.
73 R. Zafar Abbas Manj, F. Zhang, W. Ur Rehman, W. Luo and J. Yang, *Chem. Eng. J.*, 2020, **385**, 123821.
74 Y. Gao, S. Wang, H. Luo, L. Dai, C. Cao, Y. Liu, Z. Chen and M. Kanehira, *Energy Environ. Sci.*, 2012, **5**, 6104–6110.
75 J. Zhu, Y. Zhou, B. Wang, J. Zheng, S. Ji, H. Yao, H. Luo and P. Jin, *ACS Appl. Mater. Interfaces*, 2015, **7**, 27796–27803.
76 Y. Chen, Z. Shao, Y. Yang, S. Zhao, Y. Tao, H. Yao, H. Luo, X. Cao and P. Jin, *ACS Appl. Mater. Interfaces*, 2019, **11**, 41229–41237.
77 L. Mao and C. Liu, *Mater. Res. Bull.*, 2008, **43**, 1384–1392.
78 P. Liu, K. Zhu, Y. Gao, Q. Wu, J. Liu, J. Qiu, Q. Gu and H. Zheng, *CrystEngComm*, 2013, **15**, 2753–2760.
79 S.-Y. Li, K. Namura, M. Suzuki, G. A. Niklasson and C. G. Granqvist, *J. Appl. Phys.*, 2013, **114**, 033516.
80 K. C. Kam and A. K. Cheetham, *Mater. Res. Bull.*, 2006, **41**, 1015–1021.
81 A. Huang, Y. Zhou, Y. Li, S. Ji, H. Luo and P. Jin, *J. Mater. Chem. A*, 2013, **1**, 12545–12552.
82 W. Li, S. Ji, G. Sun, Y. Ma, H. Guo and P. Jin, *New J. Chem.*, 2016, **40**, 2592–2600.
83 R. Li, S. Ji, Y. Li, Y. Gao, H. Luo and P. Jin, *Mater. Lett.*, 2013, **110**, 241–244.
84 Y. Li, S. Ji, Y. Gao, H. Luo and M. Kanehira, *Sci. Rep.*, 2013, **3**, 1370.
85 T. D. Vu, H. Xie, S. Wang, J. Hu, X. Zeng and Y. Long, *Mater. Today Energy*, 2022, **26**, 100978.
86 T. Chang, Y. Zhu, J. Huang, H. Luo, P. Jin and X. Cao, *Sol. Energy Mater. Sol. Cells*, 2021, **219**, 110799.
87 H. Zhou, J. Li, Y. Xin, X. Cao, S. Bao and P. Jin, *J. Mater. Chem. C*, 2015, **3**, 5089–5097.
88 H. Kim, Y. Kim, T. Kim, A. R. Jang, H. Y. Jeong, S. H. Han, D. H. Yoon, H. S. Shin, D. J. Bae, K. S. Kim and W. S. Yang, *Nanoscale*, 2013, **5**, 2632–2636.
89 H. Li, H. Djaoued, J. Robichaud and Y. Djaoued, *J. Mater. Chem. C*, 2020, **8**, 11572–11580.
90 S. Li, Y. Li, K. Qian, S. Ji, H. Luo, Y. Gao and P. Jin, *ACS Appl. Mater. Interfaces*, 2014, **6**, 9–13.
91 W. Li, S. Ji, K. Qian and P. Jin, *J. Colloid Interface Sci.*, 2015, **456**, 166–173.
92 J. Zhou, Y. Gao, Z. Zhang, H. Luo, C. Cao, Z. Chen, L. Dai and X. Liu, *Sci. Rep.*, 2013, **3**, 3029.
93 G. Sun, X. Cao, X. Gao, S. Long, M. Liang and P. Jin, *Appl. Phys. Lett.*, 2016, **109**, 143903.
94 M. Maaza, K. Bouziane, J. Maritz, D. S. McLachlan, R. Swanepool, J. M. Frigerio and M. Every, *Opt. Mater.*, 2000, **15**, 41–45.
95 H. Koo, H. You, K.-E. Ko, O. J. Kwon, S.-H. Chang and C. Park, *Appl. Surf. Sci.*, 2013, **277**, 237–241.
96 I. Takahashi, M. Hibino and T. Kudo, *Jpn. J. Appl. Phys.*, 2001, **40**, 1391–1395.
97 L. Kang, Y. Gao and H. Luo, *ACS Appl. Mater. Interfaces*, 2009, **1**, 2211–2218.
98 M. Kumar, J. P. Singh, K. H. Chae, J. Park and H. H. Lee, *Superlattices Microstruct.*, 2020, **137**, 106335.
99 B. Li, J. Liu, S. Tian, B. Liu, X. Yang, Z. Yu and X. Zhao, *Ceram. Int.*, 2020, **46**, 2758–2763.
100 X. P. Zhao, S. A. Mofid, T. Gao, G. Tan, B. P. Jelle, X. B. Yin and R. G. Yang, *Mater. Today Phys.*, 2020, **13**, 100205.
101 J. Sang, W. Zhu, Y. Feng, Y. Liu, J. Shang, J. Sun, L. Guo, Y. Zhang, S. Zhao, V. Chigrinov and D.-S. Seo, *ACS Appl. Electron. Mater.*, 2021, **3**, 4882–4890.
102 Z. Qu, L. Yao, S. Ma, J. Li, J. He, J. Mi, S. Tang and L. Feng, *Sol. Energy Mater. Sol. Cells*, 2019, **200**, 109920.
103 X. Lv, Y. Cao, L. Yan, Y. Li and L. Song, *Appl. Surf. Sci.*, 2017, **396**, 214–220.
104 C. Nakamura, K. Manabe, M. Tenjimbayashi, Y. Tokura, K.-H. Kyung and S. Shiratori, *ACS Appl. Mater. Interfaces*, 2018, **10**, 22731–22738.
105 L. Zhou, M. Hu, X. Song, X. Qiang and J. Liang, *Appl. Phys. A: Mater. Sci. Process.*, 2018, **125**, 19.
106 X. Fan, G. Wei, X. Lin, X. Wang, Z. Si, X. Zhang and W. Zhao, *Matter*, 2020, **2**(6), 1582–1592.
107 S. Long, X. Cao, G. Sun, N. Li, T. Chang, Z. Shao and P. Jin, *Appl. Surf. Sci.*, 2018, **441**, 764–772.
108 T. Chang, X. Cao, N. Li, S. Long, Y. Zhu, J. Huang, H. Luo and P. Jin, *Matter*, 2019, **1**, 734–744.
109 M. J. Powell, R. Quesada-Cabrera, A. Taylor, D. Teixeira, I. Papakonstantinou, R. G. Palgrave, G. Sankar and I. P. Parkin, *Chem. Mater.*, 2016, **28**, 1369–1376.
110 I. Top, R. Binions, C. Sol, I. Papakonstantinou, M. Holdynski, S. Gaiaschi and I. Abrahams, *J. Mater. Chem. C*, 2018, **6**, 12555–12565.
111 H. Koo, D. Shin, S.-H. Bae, K.-E. Ko, S.-H. Chang and C. Park, *J. Mater. Eng. Perform.*, 2014, **23**, 402–407.
112 Y. Ji, A. Mattsson, G. A. Niklasson, C. G. Granqvist and L. Österlund, *Joule*, 2019, **3**, 2457–2471.
113 Y. Dang, L. Zhao and J. Liu, *Ceram. Int.*, 2020, **46**, 9079–9085.
114 M. K. Shahzad, Y. Zhang, A. Raza, M. Ikram, K. Qi, M. U. Khan, M. J. Aslam and A. Alhazaa, *Nanoscale Res. Lett.*, 2019, **14**, 270.
115 I. Top, R. Binions, M. E. A. Warwick, C. W. Dunnill, M. Holdynski and I. Abrahams, *J. Mater. Chem. C*, 2018, **6**, 4485–4493.
116 X. Zhou, Y. Meng, T. D. Vu, D. Gu, Y. Jiang, Q. Mu, Y. Li, B. Yao, Z. Dong, Q. Liu and Y. Long, *J. Mater. Chem. A*, 2021, **9**, 15618–15628.
117 H. Zhou, J. Li, S. Bao, J. Li, X. Liu and P. Jin, *Appl. Surf. Sci.*, 2016, **363**, 532–542.
118 J. Zhang, J. Wang, C. Yang, H. Jia, X. Cui, S. Zhao and Y. Xu, *Sol. Energy Mater. Sol. Cells*, 2017, **162**, 134–141.
119 S. Loquai, B. Baloukas, J. E. Klemberg-Sapieha and L. Martinu, *Sol. Energy Mater. Sol. Cells*, 2017, **160**, 217–224.
120 N. R. Mlyuka, G. A. Niklasson and C. G. Granqvist, *Sol. Energy Mater. Sol. Cells*, 2009, **93**, 1685–1687.
121 N. R. Mlyuka, G. A. Niklasson and C. G. Granqvist, *Phys. Status Solidi A*, 2009, **206**, 2155–2160.
122 Y. Zhan, X. Xiao, Y. Lu, Z. Cao, S. Qi, C. Huan, C. Ye, H. Cheng, J. Shi, X. Xu and G. Xu, *Surf. Interfaces*, 2017, **9**, 173–181.

123 M. J. Miller and J. Wang, *Sol. Energy Mater. Sol. Cells*, 2016, **154**, 88–93.
124 H. Liu, H. Song, H. Xie and G. Yin, *Eur. Phys. J.: Appl. Phys.*, 2019, **88**, 30301.
125 Y. Zhan, X. Xiao, Y. Lu, Z. Cao, S. Qi, C. Huan, H. Cheng, J. Shi and G. Xu, *Sol. Energy Mater. Sol. Cells*, 2018, **174**, 102–111.
126 Y. Zhao, R. Xu, X. Zhang, X. Hu, R. J. Knize and Y. Lu, *Energy Build.*, 2013, **66**, 545–552.
127 L. Kang, Y. Gao, Z. Chen, J. Du, Z. Zhang and H. Luo, *Sol. Energy Mater. Sol. Cells*, 2010, **94**, 2078–2084.
128 H. Liu, H. Zong, L. Yan, D. Zhou, Y. Yin, G. Cao, L. Bian, C. Kang and M. Li, *Infrared Phys. Technol.*, 2021, **113**, 103648.
129 S. Li, C. Lv, X. Lin, G. Wei, Y. Xiong, W. Yang and W. Zhao, *Appl. Phys. Lett.*, 2021, **119**(12), 122401.
130 L. Zhou, M. Hu, X. Song, P. Li, X. Qiang and J. Liang, *Appl. Phys. A: Mater. Sci. Process.*, 2018, **124**, 505.
131 H. Zong, D. Zhou, L. Yan, H. Liu, J. Wu, Q. Hu, C. Kang and M. Li, *Appl. Phys. A: Mater. Sci. Process.*, 2021, **127**, 472.
132 C. Guo, Z. Zhang, Y. Wu, Y. Wang, G. Ma, J. Shi and Y. Zhao, *Supercond. Sci. Technol.*, 2022, **35**, 075014.
133 Y. Chen, L. Fan, Q. Fang, W. Xu, S. Chen, G. Zan, H. Ren, L. Song and C. Zou, *Nano Energy*, 2017, **31**, 144–151.
134 Q. He, Y. Wang, Y. Zhou, M. He, R. Xu, S. Hu, W. Wu and R. Wang, *Opt. Mater.*, 2019, **97**, 109367.
135 H. Zong, D. Zhou, L. Yan, M. Li, W. Qiao, S. Zhang, Q. Hu and L. Bian, *Ceram. Int.*, 2022, **48**, 6734–6744.
136 S. Long, X. Cao, N. Li, Y. Xin, G. Sun, T. Chang, S. Bao and P. Jin, *Sol. Energy Mater. Sol. Cells*, 2019, **189**, 138–148.
137 T. Chang, X. Cao, L. R. Dedon, S. Long, A. Huang, Z. Shao, N. Li, H. Luo and P. Jin, *Nano Energy*, 2018, **44**, 256–264.
138 S. Long, H. Zhou, S. Bao, Y. Xin, X. Cao and P. Jin, *RSC Adv.*, 2016, **6**, 106435–106442.